UNIVERSITY
OF OSLO

# Magnetic Susceptibility Artefact Correction of Spin-Echo and Gradient-Echo EPI Images

Gary McGinley

University of Oslo

Department of Physics

# Preface

This thesis is a part of my Master's degree in Biophysics and Medical Physics at the University of Oslo. This project was carried out in collaboration with the Intervention Centre at Oslo University Hospital.

# Contents

# 1 Abstract

Distortion and other artefacts caused by an uneven magnetic field affect MR images acquired with the rapid technique echo-planar imaging (EPI). This study investigates the effectiveness of reverse gradient susceptibility correction methods on spin echo (SE) and gradient echo (GE) EPI. In addition, the effects of varying bandwidth, SENSE factor and slice thickness on the corrected images were measured. Undistorted, anatomically accurate images are necessary in relating EPI images to anatomical MRI scans. This is particularly important for diffusion weighted imaging, perfusion imaging and fMRI. Due to the ever-increasing need for better temporal resolution with existing hardware, effective artefact correction in post-processing is necessary, as is appropriate sequence optimisation. This investigation was accomplished using normalised mutual information to compare the images pre and post correction to an anatomical image as a measure of anatomical accuracy. It was found that the correction of geometric distortions is equally effective in GE-EPI and SE-EPI, and that geometric correction can reduce the impact of the aforementioned scan parameters on the anatomical accuracy of the images. Three correction methods were compared in this investigation; FSL TOPUP, EPI-EPIC and ACID HySCO. It was found that, in most situations, the EPIC susceptibility correction tool was the most effective tool at correcting geometric distortions without the generation of new artefacts. Susceptibility artefact corrections were also successfully conducted on 7T contrast enhanced single shot EPI images of a prostate tumour xenograft (nude mouse). These findings could help establish

clinical and research protocol for susceptibility artefact post-processing, as well as sequence optimisation.

# 2 Introduction

Echo Planar Imaging (EPI) is the fastest approach currently available to acquire an MRI image. It is as a result now utilised widely in research and in clinical investigations. It is therefore of great importance to ensure that not only are the images as clear and anatomically accurate as possible, but that the methods that we choose to achieve these ends are tested under a wide variety of conditions. The major causes of deformations and artefacts in EPI images are magnetic susceptibility artefacts.

One of the main uses for EPI is in Dynamic Susceptibility Contrast (DSC) MRI, whereby a contrast agent is introduced to a patient and a T2* weighted gradient echo (GE) EPI sequence is used to obtain images as the contrast flows through the region of interest. This method is predominantly used in the assessment of acute stroke and inter-cranial tumours. This technique, however has been shown to be underutilised for a number of reasons, one of which being the lack of standardised post-processing tools available [1]. This lack of consensus with regard to post processing tools similarly applies to tools used for the correction of susceptibility artefacts. Considering the high probability of susceptibility artefacts in these sequences, it is important that each correction method is tested and protocol can be established, particularly in clinical situations. This will ensure that geometrically accurate delineation of pathology can be derived from the EPI images.

Diffusion MRI is used to map the diffusion of water molecules within a voxel of biological tissue. Since proton motion induces phase shifts in the MR signal, when water molecules diffuse in the direction of a pulsed gradient, there will be signal loss in the voxel due to intra-voxel phase dispersion. Therefore, by acquiring EPI images with and without diffusion gradients that spoil the signal in proportion to the water diffusability, diffusion can be measured. This technique has many clinical applications, such as the identification of ischemic stroke, assessing active demyelination and, in the case of diffusion tensor imaging, assessing the integrity and connectivity of white matter [15]. In this case, susceptibility artefacts can result in distorted diffusion-tensor maps [16]

Functional MRI (fMRI) is another technique which utilises EPI imaging. In Blood-Oxygen Level Dependent (BOLD) contrast imaging, the differing magnetic properties of oxygenated and deoxygenated blood allow neural activity to be measured. This is possible because, as neural activity increases, blood oxygenation initially decreases, before blood flow to the area increases and oxygenation becomes higher than baseline levels. In BOLD fMRI, it is once again important to be able to correct susceptibility artefacts, particularly in the temporal and frontal lobes where they are most prevalent [2] [3]. It has also been shown that susceptibility artefacts reduce BOLD contrast in fMRI [14].

There have been several methods devised with which it is possible, to a greater or lesser degree, to correct susceptibility artefacts in EPI sequences, but the reverse-gradient method is regarded as the most effective [4]. In this study, three separate tools for susceptibility artefact correction were analysed and compared using double echo EPI images acquired from healthy volunteers. The double echo sequence allowed us to simultaneously acquire SE and GE EPI images and compare the distortion effects and correction efficacy of each. In addition, the effects of varying pixel bandwidth, slice thickness and SENSE factor on the severity of magnetic susceptibility artefacts were analysed.

# 3 Theory

## 3.1 Echo Planar Imaging

Echo Planar Imaging (EPI) is a pulse sequence which utilises an accelerated k-space trajectory to acquire multiple lines of k-space after the application of a single RF-excitation. The spins are re-phased in EPI sequences by using gradient echo refocusing, and therefore, due to the speed with which gradient echoes can be created in a modern MRI scanner (within a millisecond), an EPI image can be acquired in under 80 ms for a full 64 x 64 matrix k-space acquisition. The GE-EPI pulse sequence is shown below:
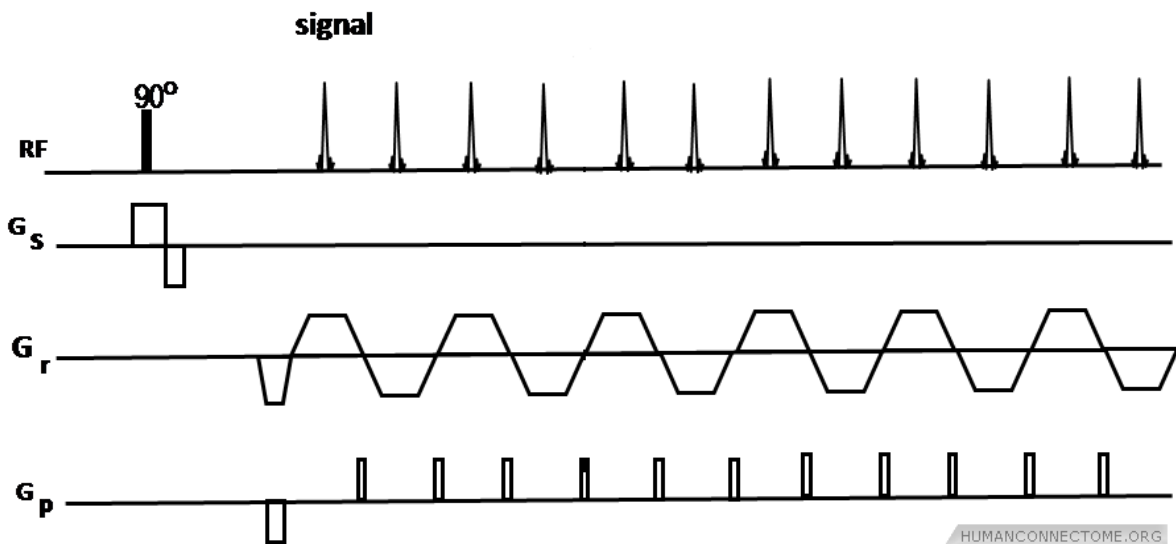


*Figure 3.11 GE-EPI pulse sequence [5], where a single excitation pulse is used to acquire multiple lines of k-space by the use of gradient echo rephasing*

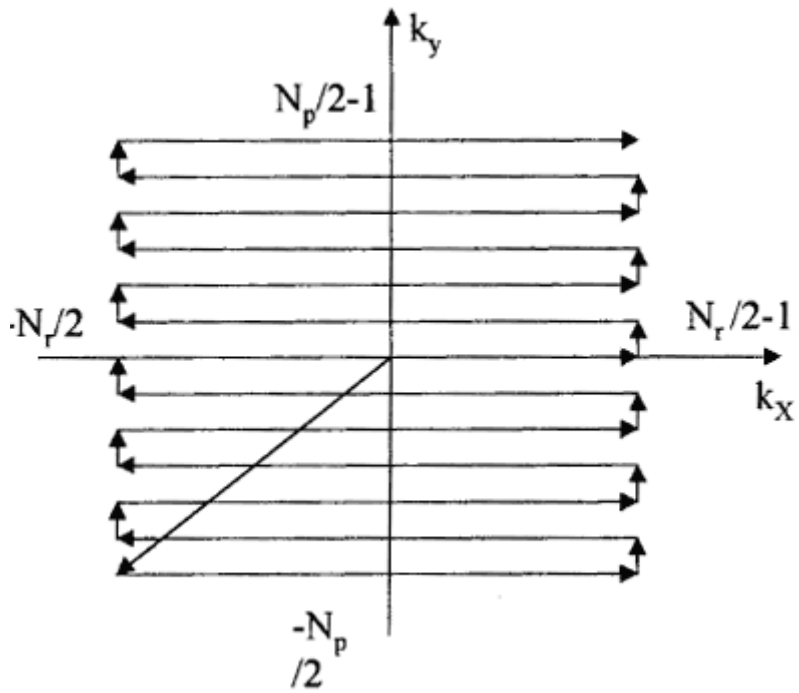The above sequence generates a rectilinear k-space trajectory as follows:

*Figure 3.12 A representation of a typical k-space trajectory for a GE-EPI pulse sequence [6]*

It is also possible to create T2 weighted spin-echo EPI sequences. This is achieved by the addition of a single 180 degree pulse prior to the EPI readout sequence, as shown below:
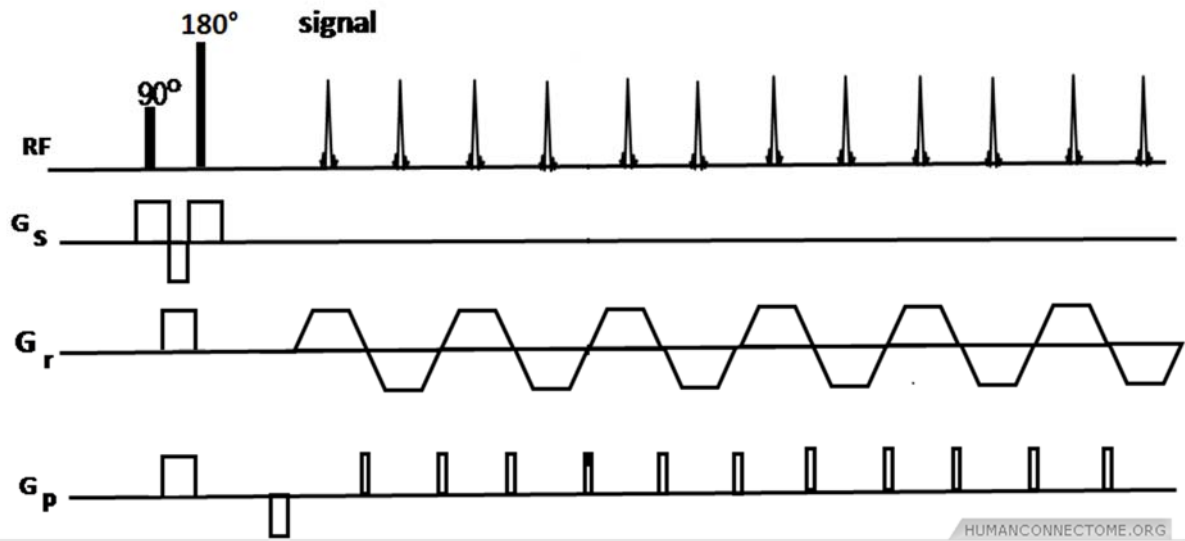
*Figure 3.12 SE-EPI pulse sequence [5], where an additional 180 degree pulse is used, providing T2 weighting*
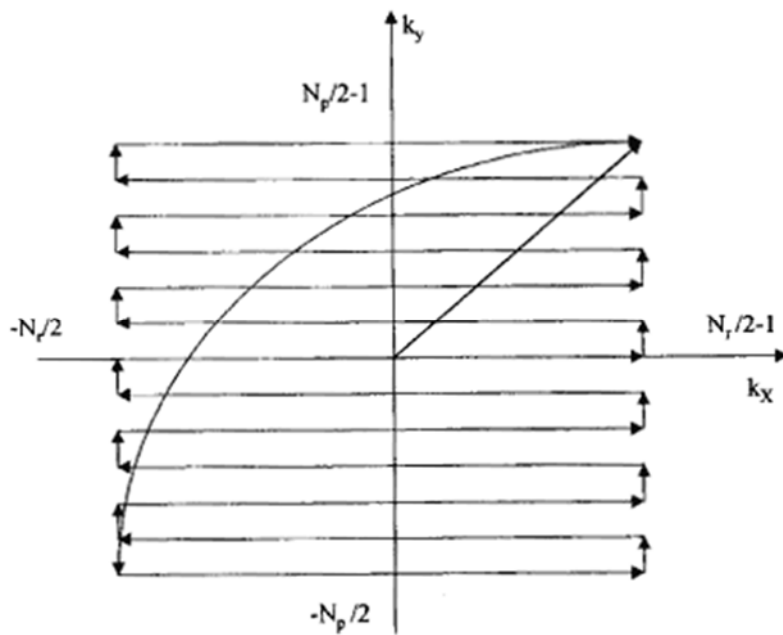
Leading to the following k-space trajectory:



*Figure 3.13 A representation of a typical k-space trajectory for an SE EPI sequence [6]*

*[6]*

## 3.2  Susceptibility Artefacts

The main disadvantage of EPI, however, is that it is extremely sensitive to artefacts. This is predominantly due to the modality's high sensitivity to inhomogeneities in the magnetic field. The methods used in this study attempt to correct magnetic susceptibility artefacts.
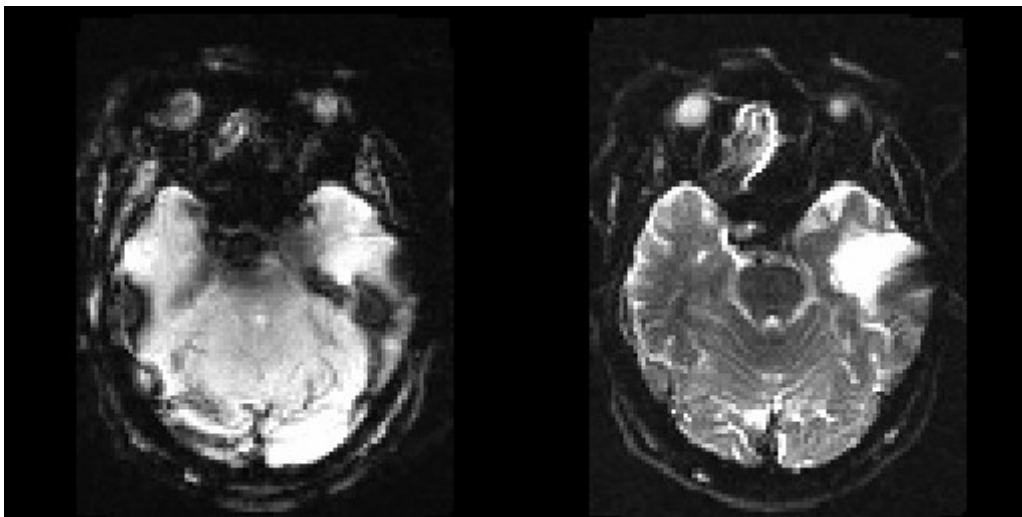


*Figure 3.20 A GE-EPI image showing susceptibility induced signal loss and geometric distortions (left) and a SE-EPI image showing geometric distortion, but less susceptibility induced signal loss. This is an example of how susceptibility artefacts can obscure regions of interest in an image. The tumour in the left temporal lobe is distorted due to susceptibility artefacts.*

Magnetic susceptibility artefacts are caused by local differences in magnetic susceptibility. These artefacts can be extremely detrimental to the image when caused by metal implants from braces for example, causing irrecoverable signal

loss. To a lesser extent, susceptibility artefacts are found at air-tissue boundaries. This is because air is paramagnetic ($\chi > 0$) and brain tissue is diamagnetic ($\chi < 0$), which induces a magnetic field gradient across the boundary, given by $\Delta \chi B_0$. These artefacts are less detrimental and can, to an extent, be corrected. In the brain, these artefacts are found near the ear cavities and near the sinuses.

T2 relaxation can be said to describe the decay of the transverse component of the magnetisation following the excitation pulse, reflecting field inhomogeneities at the molecular level due to spin-spin interactions. T2* relaxation, however, also includes the effects of bulk inhomogeneities in the field over much longer distances. Field inhomogeneities, such as those caused by differences in magnetic susceptibility, act to reduce T2*. The geometric effect of the T2* and field inhomogeneity is shown in equation 3.1:

$$\rho(x,y) = \frac{1}{2\pi} \int\limits_{k_x} \int\limits_{k_y} M_T(k_x, k_y) \exp(j(k_x + k_y y)) \exp\left(-{t}/{T2*}\right) \exp(-j\delta B(x,y)t)\, dk_x dk_y \tag{3.1}$$

The three main effects of magnetic susceptibility on the image are described below.

## 3.21 Geometric Distortion

Geometric distortions manifest themselves as pixel movements, predominantly in the phase encoding direction in EPI images. They can have the appearance of stretching or bunching of signal near in the vicinity of field inhomogeneity. In SE-EPI, T2* effects are cancelled out by the refocusing 180° pulse.

However, returning to equation 3.1, the field inhomogeneity term $\exp(-j\delta B(x,y)t)$ has an effect on both EPI methods. This term causes spatial distortions, where the shift in position of the pixels are given by [17]:

$$x' = x \pm \frac{\delta B(x,y)}{G_x} \quad \text{and} \quad y' = y + \frac{\delta B(x,y)}{G_y} \cong y + \frac{\delta B(x,y)N}{G_x} \qquad (3.2)$$

If we now wish to describe these shifts in terms of magnetic susceptibility, we need only substitute the δB value with $\Delta\chi B_0$ to get:

$$x' = x \pm \frac{\Delta\chi B_0}{G_x} \quad \text{and} \quad y' = y + \frac{\Delta\chi B_0}{G_y} \cong y + \frac{\Delta\chi B_0 N}{G_x} \qquad (3.3)$$

The spatial distortions are often negligible in the readout direction due to the much larger bandwidth, but are greatly significant in the phase-encoding direction. The pixels are therefore shifted in the direction if the phase encoding gradient.

## 3.22 Signal Loss

The transverse magnetisation is T2* dependent. The effect of field inhomogeneities is dependent upon the size of the phase dispersion caused relative to the size of the pixel. Intra-voxel dephasing is where field inhomogeneities occur within a voxel, resulting in signal loss due to phase dispersion. This type of artefact is more prevalent in GE-EPI, as the 180 degree pulse in SE-EPI acts to reverse phase dispersions and reduce dependence on T2*
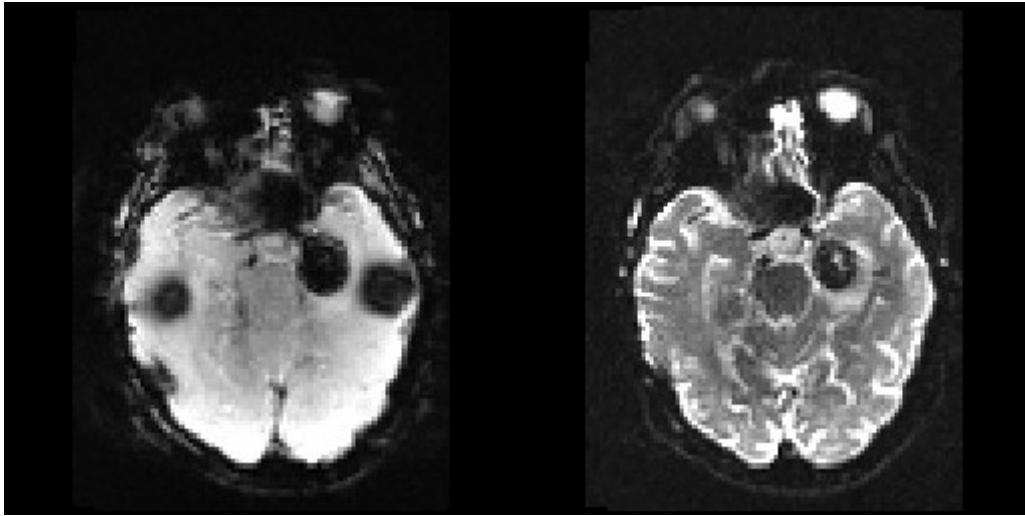
*Figure 3.21 Signal loss caused by susceptibility effects in GE-EPI (left) and geometric distortion in SE-EPI (right). The extent of the signal loss in the GE-EPI image causes the tumour to be obscured, and the signal loss could be mistaken for pathology. The SE-EPI image does not suffer from the same level of signal loss, but geometric distortion is apparent.*



*Figure 3.22 A visual representation of intra-voxel dephasing (top) and off-resonance effects (bottom)*

## 3.22 Blurring

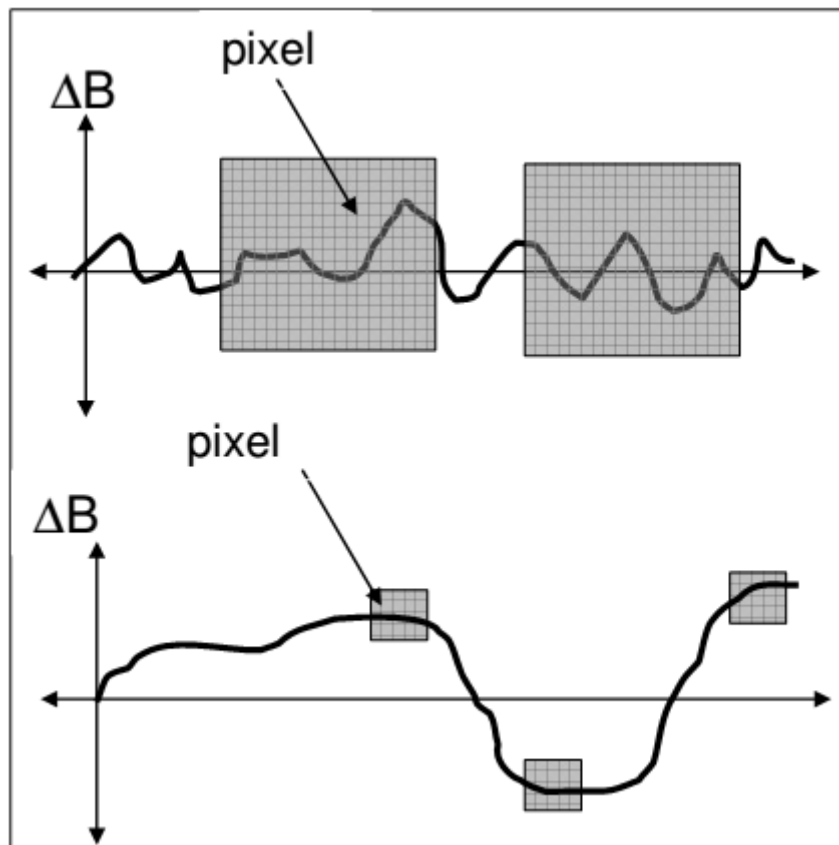The geometric effect of susceptibility can be described by adding a δB term to the standard k-space formalism as follows:

$$(3.1)$$

where ρ(x,y) is the object and δB is the field inhomogeneity [8]. As the object is convolved with the exponential T2* relaxation, the point spread function becomes a Lorentzian function (as the Fourier transform of an exponential function is a Lorentzian), leading to blurring.

The FWHM of the point spread function is given by[18]:

$$\Delta x = 2/(\gamma \langle G \rangle T_2^*) \qquad (3.2)$$

As this is dependent upon the average gradient, the blurring due to T2* in the readout direction is minimal, due to the strong effective gradient. In the phase direction, however, the effective gradient is much lower, as k-space is traversed much more slowly in the phase encoding direction. If $k_y$ is taken to represent k-space in the phase encoding direction, then the k-space velocity in the phase encoding direction is given by $v_y = \frac{t}{k_y(t)}$, where $v_y$ can be approximated as $v_x/N$, where N is the number of lines of $k_y$ lines acquired. This results in a pseudo-gradient a factor of approximately N smaller than in the phase encoding direction, leading to a larger degree of blurring.
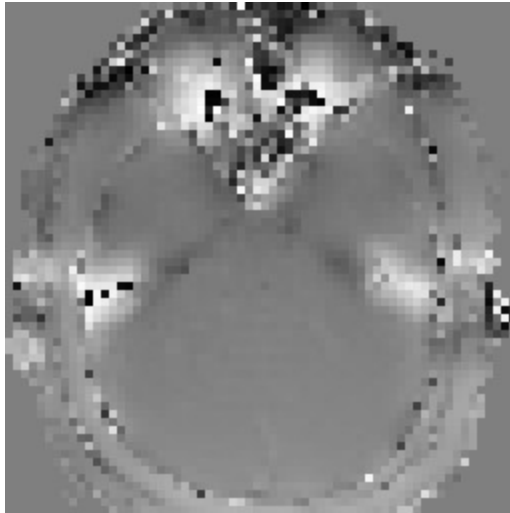
## 3.3  Susceptibility correction methods

### 3.31 Field map correction

There are several methods for attempting to correct susceptibility artefacts in EPI images. A simple method for unwarping these images are "field map"-based corrections. This is where a map of the background magnetic field inhomogeneity acquiring two complex gradient echo images with different echo times and by determining their phase difference. The field inhomogeneity can be calculated from the phase difference using the relation [7]:

$$\Delta\phi = -\gamma\Delta B(r)\Delta TE \tag{3.5}$$

This map can be used to calculate the pixel shift due to the inhomogeneities and therefore be used to correct these distortions. This method has various limitations due to the difficulty of calculating the phase difference in areas where the field inhomogeneity is high, challenges regarding phase unwrapping, and the lack of voxel intensity information. The scan sequences required to obtain the phase map also takes several minutes to acquire, as opposed to the few seconds it takes to acquire an EPI scan of an entire brain, therefore subject motion during the former can lead to large errors in the field map and subsequent correction.

*Figure 3.30 Example of a B0 map acquired from the volunteer study*

## 3.32 PSF unwarping

Another method of susceptibility distortion correction is point spread function (PSF) unwarping. The theory behind this method is that the measured image is the convolution of undistorted image and the PSF, and therefore by mapping the PSF, one can calculate the undistorted image by deconvolution [8]. This is achieved by taking many single shot EPI scans per slice, and before each acquisition applying a preparatory phase encoding gradient with a different gradient strength. These gradients together provide a complimentary set of $k_y$ points per data point acquired and allows the measurement of the PSF for each voxel individually. This technique is less fragile than the field map method, but suffers similarly from a long acquisition time due to the large number of EPI scans necessary to obtain the PSF map.

## 3.33 Reversed gradient method

The method employed in all three of the programs used in this study is the reversed gradient method [7, 8, 9, 10, 11, 12]. This is where EPI scans are taken with opposing phase encoding directions, which, as a result, have distortions that are reversed with respect to the pixel shift direction along the phase encode direction. It is therefore possible to extract the undistorted image from this by finding a midpoint between the distortions obtained in each acquisition. This is achieved by setting up a least squares cost function to attempt to find the correct displacements in the phase encoding direction to match the two opposite polarity images as closely as possible. This involves:

1. Creating an initial displacement map, where the displacement field equals zero and the standard deviation of the smoothing kernel is chosen.
2. The forward and reverse phase-encoded images must be smoothed
3. One iteration of the cost function is then run calculated, producing an approximation of the displacement field
4. The images are updated, and the smoothing is lowered by a set increment

This process is then repeated until the forward and reverse images fit the given programs criteria for similarity, i.e. the cost function is minimised.

The initial level of smoothing is dependent on the magnetic field strength, so should be higher for 3T images than for 1.5T images. This allows estimates for global minima to be calculated which can be used to apply the cost function to the images with less smoothing. This prevents large, perhaps erroneous, displacements from being included in the final correction.

Once the displacement map is obtained for two volumes with opposite phase polarity, the same correction can be applied to an entire dynamic series. As only

a single image with opposite phase polarity is required to estimate the displacement, the additional scantime required to obtain corrected images is very low in comparison to generating a B0 map.
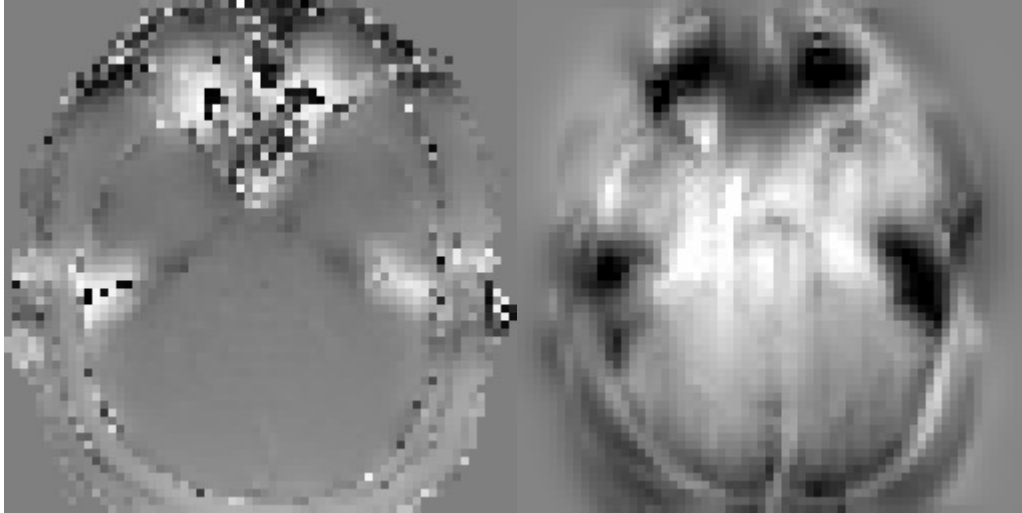


*Figure 3.31 Comparison of the measured B0 map (left) and the calculated fieldmap in the same slice from EPIC(right) The calculated fieldmap tends account for extreme inhomogeneities more accurately*

## 3.5  Scan parameters and susceptibility

In this study, we focus on three parameters that are expected do have a significant impact on geometric EPI artefacts; pixel bandwidth, slice thickness and SENSE factor. The effects of these factors were investigated in both GE and SE EPI images.

### 3.51 Pixel bandwidth

The pixel bandwidth determines how magnetic susceptibility artefacts present in the image. If the voxel dimension is large with respect to the field perturbation, intra-voxel dephasing occurs. This is where the spins within a voxel de-phase, resulting in signal loss in that voxel. In the case of the bandwidth being low

with respect to the inhomogeneity in the field, the voxel will instead be geometrically distorted, i.e. moved in the direction of the gradient created by the difference in susceptibility (see figure 3.22).

## 3.52 Slice thickness

The voxel volume is another factor determining whether intra-voxel dephasing or geometric distortions occur. By increasing the slice thickness, the voxel volume is increased, reducing the extent of geometric distortions [1].

## 3.53 SENSE factor

SENSitivity Encoding, or SENSE is a method of parallel imaging used for accelerating acquisition. It reduces the amount of k-space data obtained by a chosen value. A value of one would mean all lines of k-space are acquired, whereas a value of two would mean only half were acquired. The decrease in acquisition time allows either the same information to be acquired in a shorter time, or an increase in the image resolution over the same time when compared to a non-parallel imaging sequence. Parallel imaging also results in a reduced echo train length, therefore reducing the build-up of artefacts before reconstruction. The omitted phase encodings lines in k-space, result in the image becoming aliased, and therefore must be reconstructed using known coil sensitivity profiles. Susceptibility artefacts can interfere with this reconstruction [19]. As a result, with increasing SENSE factor, it is possible that a wide variety of artefacts can result from incorrect reconstruction. This would suggest that the artefacts obtained by choosing a lower SENSE factor should be correctable with the means employed in this experiment, whereas the less predictable reconstruction artefacts may not be.

## 3.6 Co-registration

Co-registration involves taking two images and geometrically registering them, before transforming one to the others spatial orientation. In SPM [22], the tool we have used for co-registration, this is accomplished by first, performing an affine registration. There are twelve parameters involved, a translation, rotation, zoom and shear transform for each dimension, which ensures that the shape and size of the structures in the image are aligned. This is accomplished by using an algorithm to minimise:

- the mean squared difference between the images
- the squared distance between the image parameters

In this case, the cost function utilised Normalised Mutual Information (NMI) to complete the affine transform, which calculates the similarity of a joint distribution. A pixel-wise comparison of the images is made, a value of mutual information is calculated (always above 1, the higher the value, the more mutual information), and a transformation is made that is expected to increase this value. When this value is maximised, the co-registration is complete. Normalised mutual information is considered the standard for cross-modality co-registration.

# 4 Materials and Methods

## 4.1 Correction Tools

### 4.11 TOPUP

The first of the correction tools utilised in this study was FSL's [25] TOPUP [9]. Like all of the correction tools discussed in this paper, TOPUP takes images acquired with opposing phase encoding directions and estimates a field that is in turn used to correct the images. To do this, TOPUP iteratively suggests a field which it then uses to correct the images and then evaluates the corrected images. It repeats this process until the similarity between the two corrected images is maximised. It measures this similarity by taking the sum-of-squared differences of the pair of unwarped volumes, which then allows TOPUP to find the field and movement between the image acquisitions by use of the Gauss-Newton algorithm. TOPUP unfortunately destroys the top and bottom slices of the corrected image volume. To avoid this, additional duplicate slices can be added to the top and bottom of the input images, which can then be removed from the corrected image. Information on the use of TOPUP can be found in Appendix 1.

## 4.12 EPIC

The second correction program used was EPI-EPIC [7]. The correction algorithm is very similar to that of FSL's TOPUP, in that two images are compared and the voxel movement required for both images to match is calculated using a least-squares cost function. This function is then minimised with steadily reducing levels of smoothing. The smoothing helps in avoiding local minima in the calculation of the global minimum. Information on the use of EPIC can be found in Appendix 2.

## 4.13 HySCO

The third and final correction program used was HySCO. HySCO stands for "Hyper-elastic susceptibility artefact correction of diffusion weighted images [12]. This is part of the ACID toolbox, which contains software plugins for SPM, and therefore can be installed by extracting the ACID scripts into the plugins subfolder in the SPM folder. This, once again is a reverse gradient method, where the main difference seems to be the use of an additional nonlinear regularisation term. This accounts for differences in intensity between the images and ensures that the transformations are diffeomorphic i.e. the function is invertible, and both the function and its inverse are smooth. Information on the use of HySCO can be found in Appendix 3.

## 4.2  Imaging Protocol

Five healthy volunteers were scanned on a 3T Philips Achieva MRI system with an 8-channel SENSE head coil for all of the imaging data used to test the correction methods. A T1 weighted sagittal full head scan was acquired, which was used for the anatomical reference for co-registration, a B0-map was acquired to compare with the displacement maps generated by the correction methods, and GE-EPI and SE-EPI images were acquired. The default scan parameters for the EPI sequences were as follows:

TR = 1500ms

TE = 35ms

FOV = 192

Echo Train length (ETL) = 62

with varying pixel bandwidths in the PE direction:

Low = 636 Hz

Medium = 893 Hz

High = 1861 Hz

Slice thickness was varied, with values of 2mm, 4mm and 6mm, and the SENSE factor in the phase encoding direction was varied with values one, two and three.

## 4.3  Animal Scanner

Images from a Bruker Biospin 7T BioSpec animal research scanner were also corrected in the course of this project. This is mainly used as an example to show that the reverse gradient method for image correction can correct warps and gain mutual information from images acquired with a higher magnetic field strength. As shown before, magnetic susceptibility artefacts scale with $B_0$, and therefore are more detrimental to images acquired from a 7T scanner than a 3T scanner.

Two single shot EPI images with opposing phase-encoding direction were acquired alongside a multi-shot EPI sequence which was used as the template for co-registration used to acquire the NMI values for the corrected and uncorrected images. The tissue imaged is of a nude mouse with a prostate cancer xenograft.

## 4.4  Statistical Tests

To determine the statistical significance of the differences between NMI and pixel bandwidth, SENSE factor and Slice Thickness, both Kruskal-Wallis and Mann-Whitney nonparametric analysis were used, with a confidence value of 95% (p=0.05).

# 5 Results

## 5.1 Correction tool comparison

The mean NMI and standard deviations of the original and corrected images of each correction method are shown in Figure 5.1
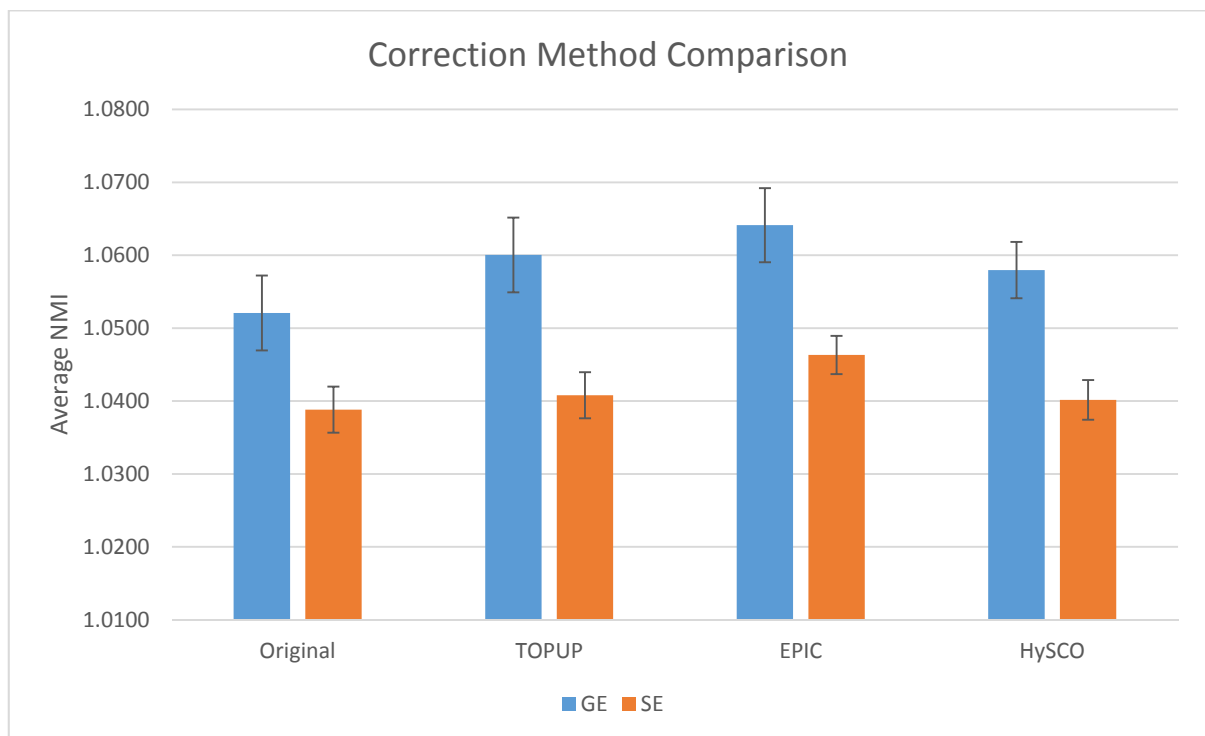


*Figure 5.10 Average NMI of the uncorrected and corrected images for each correction method for both GE-EPI and SE-EPI images.*

The change in mutual information after correction was found to be significant for only the EPIC correction method, according to the Mann-Whitney u-test. EPIC sees the most significant gains in terms of mutual information, with TOPUP and HySCO showing almost equal results. These results were obtained without the addition of empty or duplicate slices to the input images provided to TOPUP. The TOPUP corrections were repeated with duplicate slices, but this had no measurable impact on the correction.

The EPIC correction was shown to give significantly higher change in NMI according to the Kruskal-Wallis test. The standard deviation in the change in NMI for the HySCO correction was very high. Many HySCO corrected images lost mutual information, hence the low average NMI. The TOPUP correction also resulted in mutual information loss in some cases, particularly when correcting SE-EPI images.
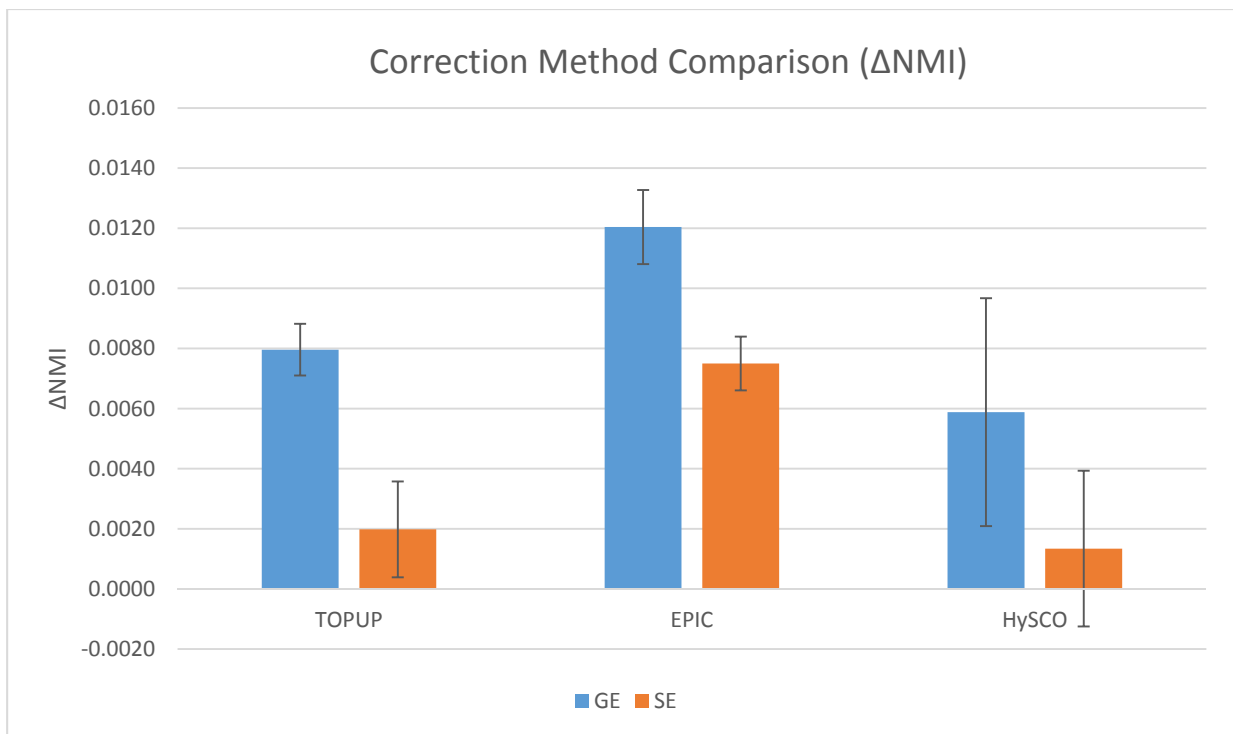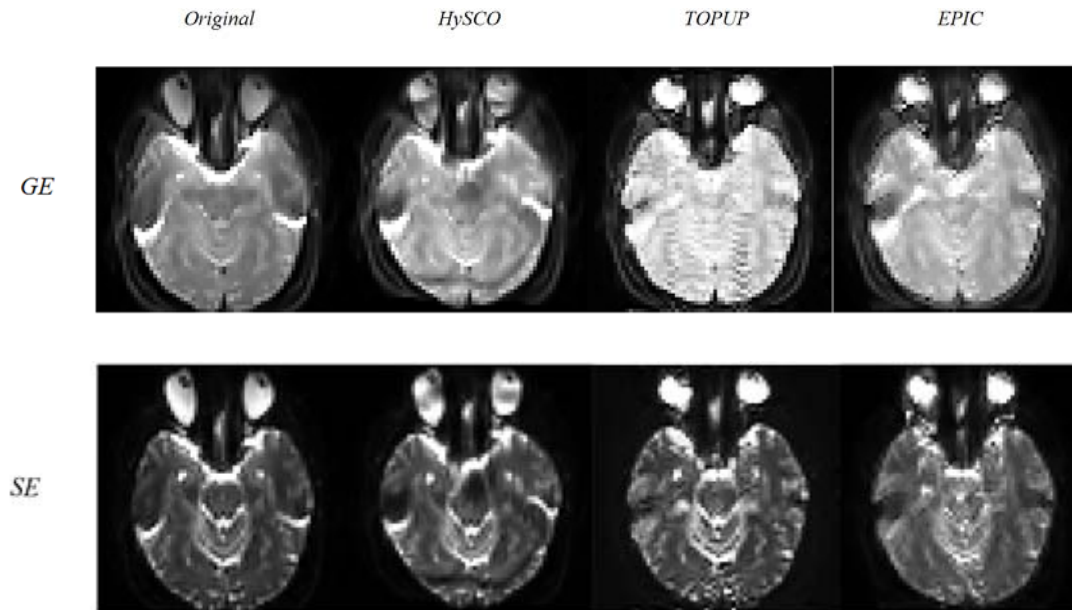


*Figure 5.11 The change in NMI for each correction type in GE and SE-EPI*

*Figure 5.12 A comparison of the three correction methods in Gradient and Spin Echo EPI. These images are from the dataset with medium bandwidth, SENSE factor 2 and a slice thickness of 4mm.*
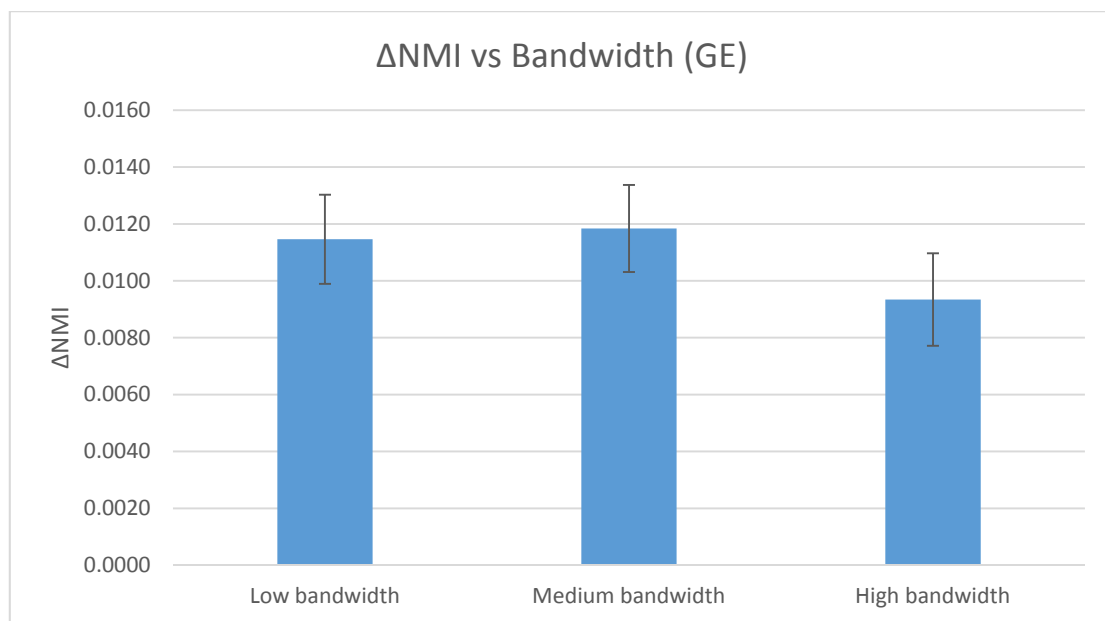
## 5.2 Bandwidth

The normalised mutual information values in figure 5.20 tend towards increasing NMI with increasing bandwidth when the corrected and uncorrected images were compared with anatomical images. This data was found by calculating the mean NMI for all uncorrected GE images and all corrected GE images separately for each of the 3 different bandwidths selected for investigation. As the most successful correction method, as shown above, EPIC was used as the correction method to obtain these results. The difference in average NMI for varying bandwidth in our GE-EPI images was found to be insignificant according to Kruskal Wallis.
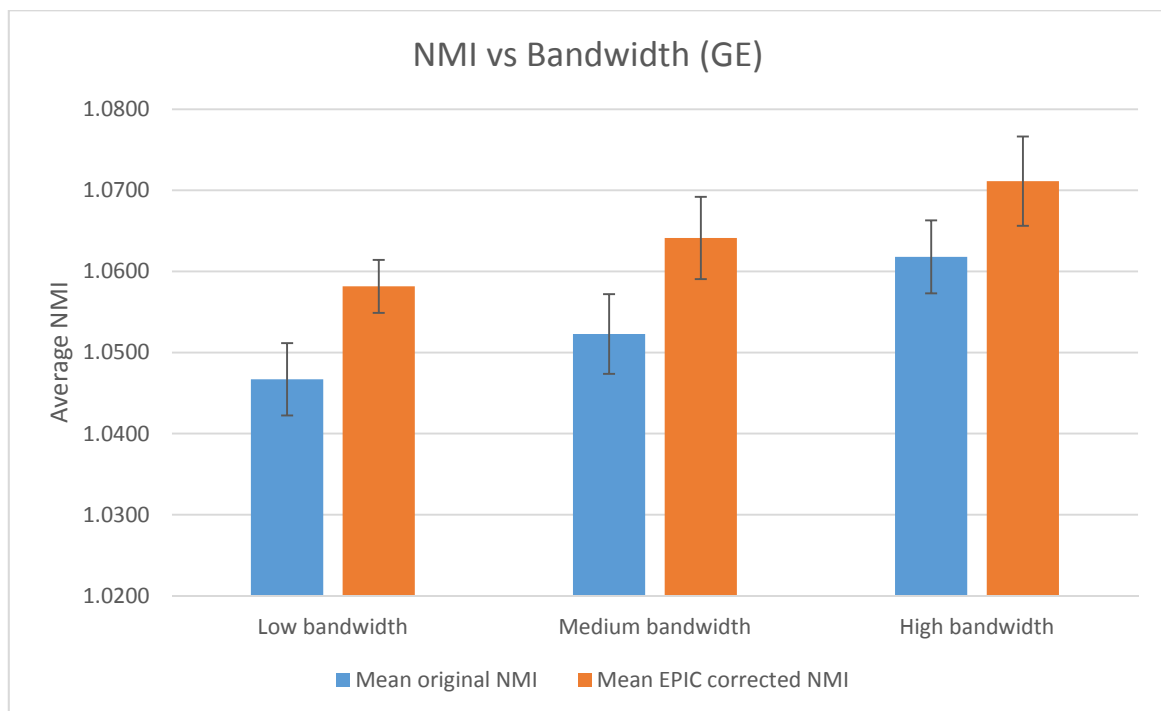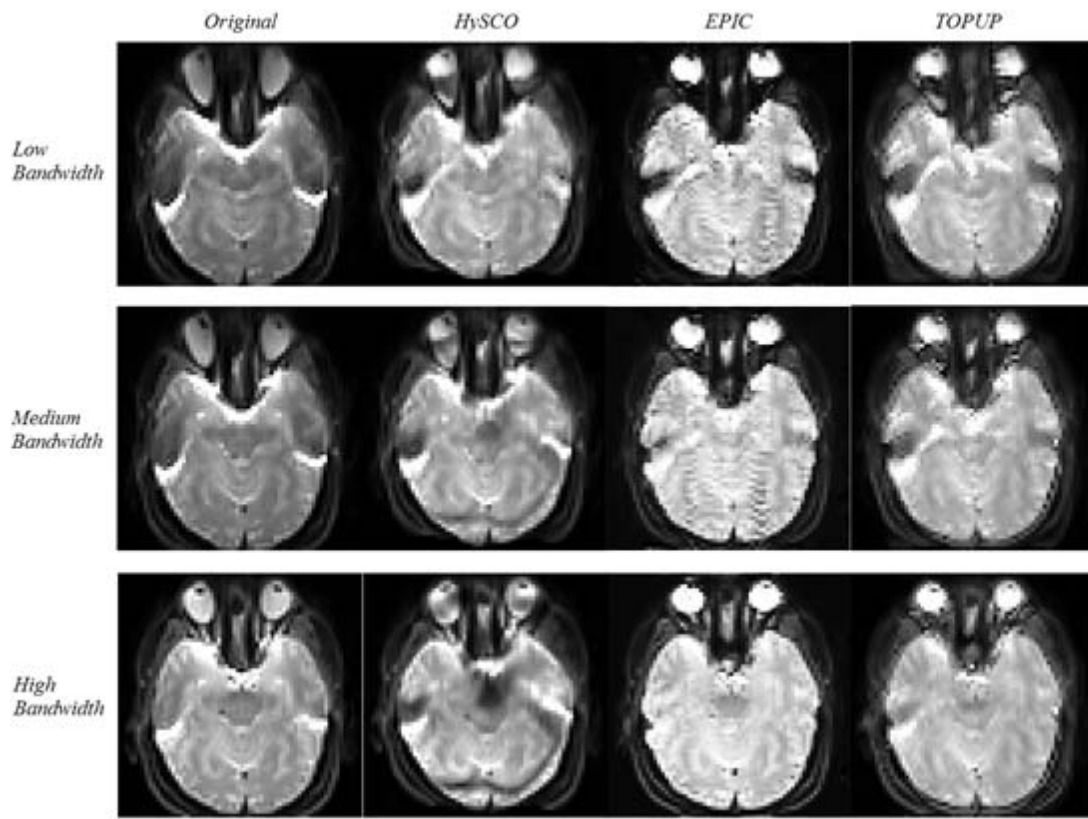


*Figure 5.20 The average NMI of GE-EPI images, before and after EPIC correction with varying bandwidth*

While the NMI was higher for the high bandwidth images, it was found also that images of lower bandwidth saw more significant gains in mutual information after correction, with an optimal increase obtained at our medium bandwidth. The Kruskal-Wallis test showed no significant difference between the three groups



*Figure 5.21 The change in NMI of GE-EPI images after EPIC correction with varying bandwidth*

*Figure 5.22 A comparison of the three correction methods using GE-EPI images of varying bandwidth.*

The same comparison was made with the SE images, and the same correlation was found as shown in figure 5.23
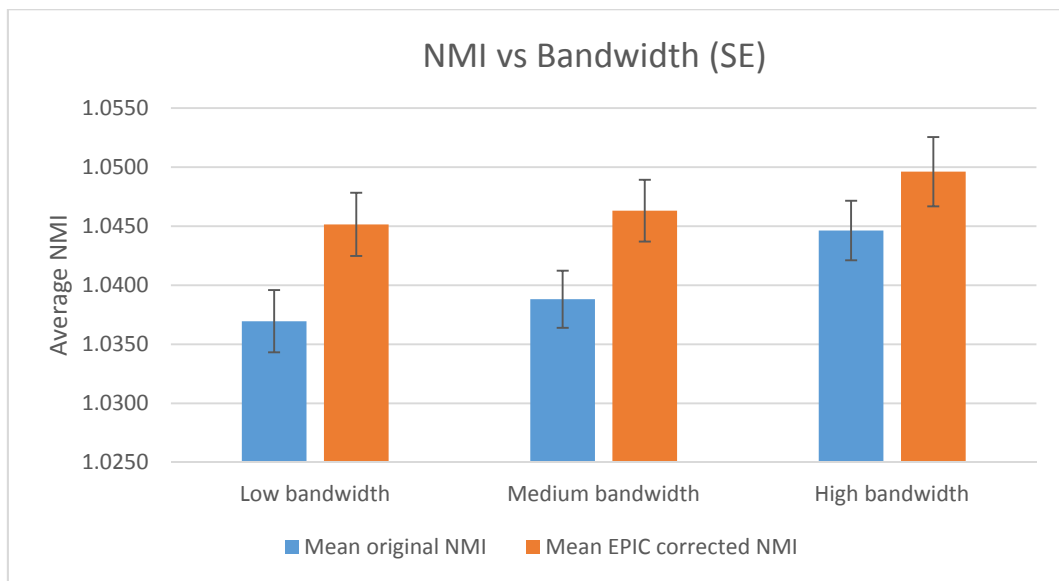


*Figure 5.23 The average NMI of SE-EPI images, before and after EPIC correction with varying bandwidth*

In the case of the SE images, it was found that the change in the NMI value for each value of bandwidth was significant according to the Kruskal-Wallis test.
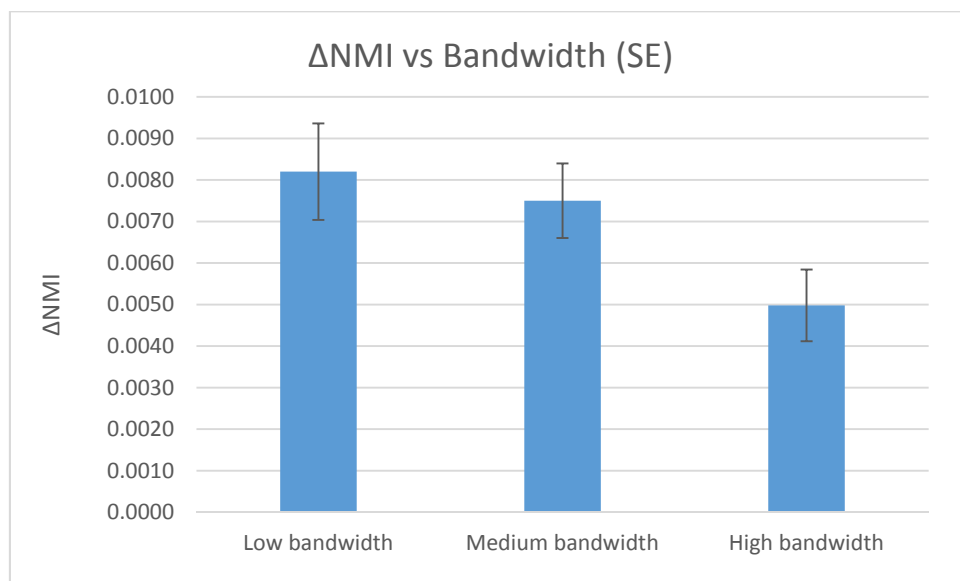
*Figure 5.24 The change in NMI of SE-EPI images after EPIC correction with varying bandwidth*



*Figure 5.25 A comparison of the three correction methods using SE-EPI images of varying bandwidth.*

## 5.3 SENSE Factor

The relationship between SENSE factor and NMI in the corrected and uncorrected images was found to be statistically insignificant in GE-EPI.



*Figure 5.30 The average NMI of GE-EPI images, before and after EPIC correction with varying SENSE factor*

The differences in the change in mutual information with respect to SENSE factor in GE-EPI were significant according to the Kruskal-Wallis test.

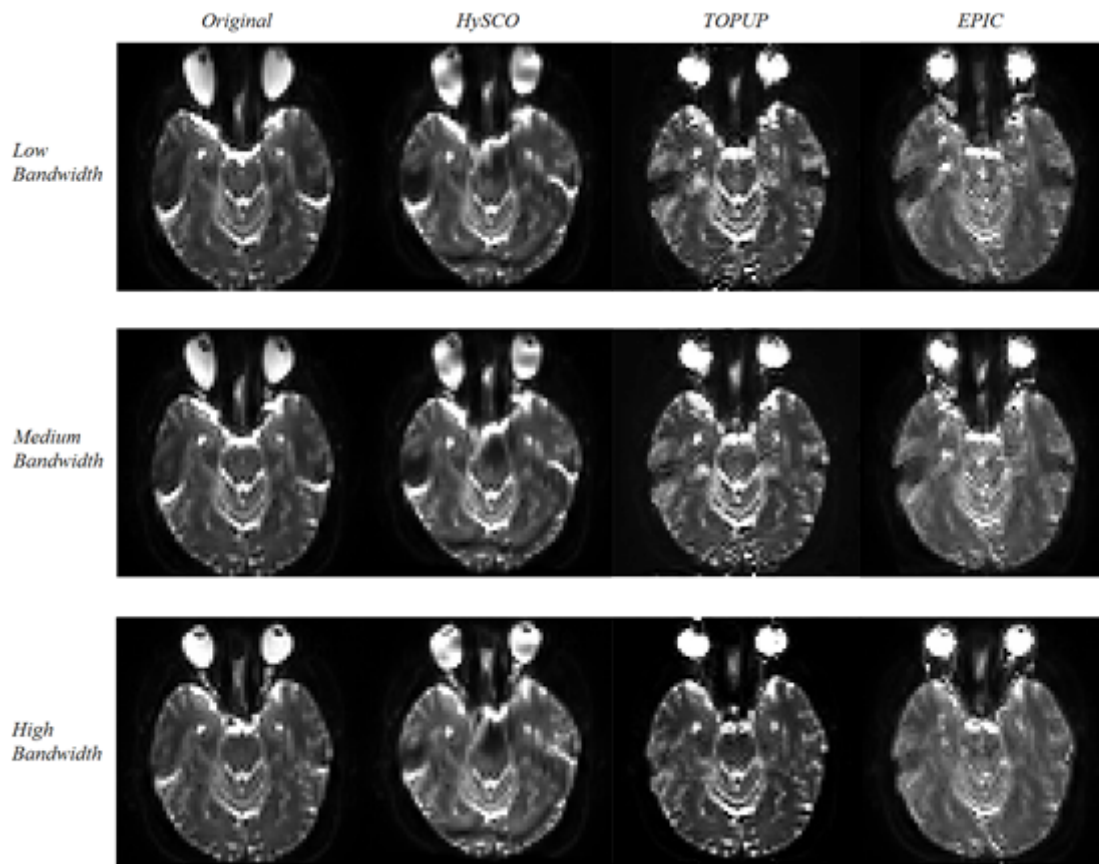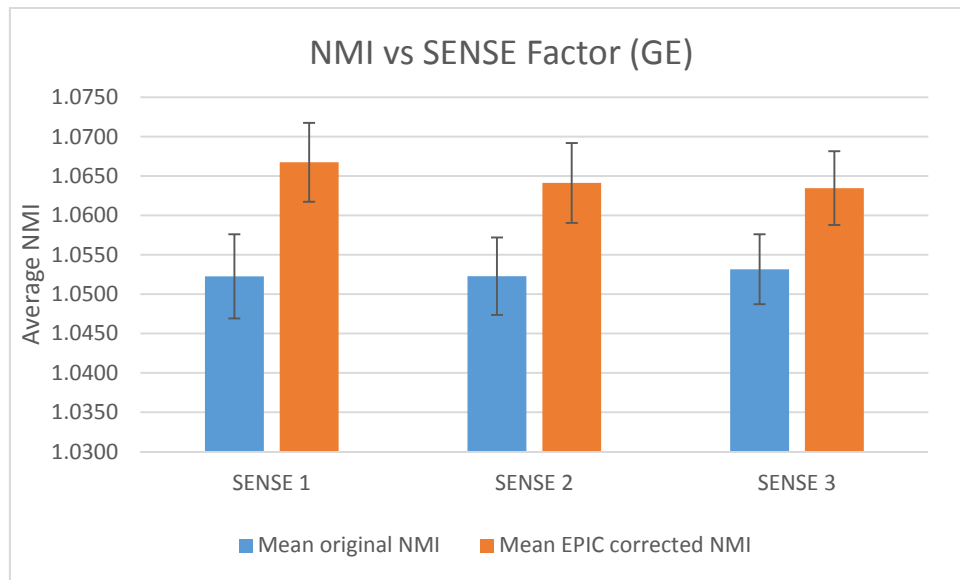*Figure 5.31 The change in NMI of GE-EPI images after EPIC correction with varying bandwidth*



*Figure 5.32 A comparison of the three correction methods using GE-EPI images of varying SENSE factor.*

For the SE-EPI images, the relationship between SENSE factor and NMI was statistically insignificant according to the Kruskal-Wallis test
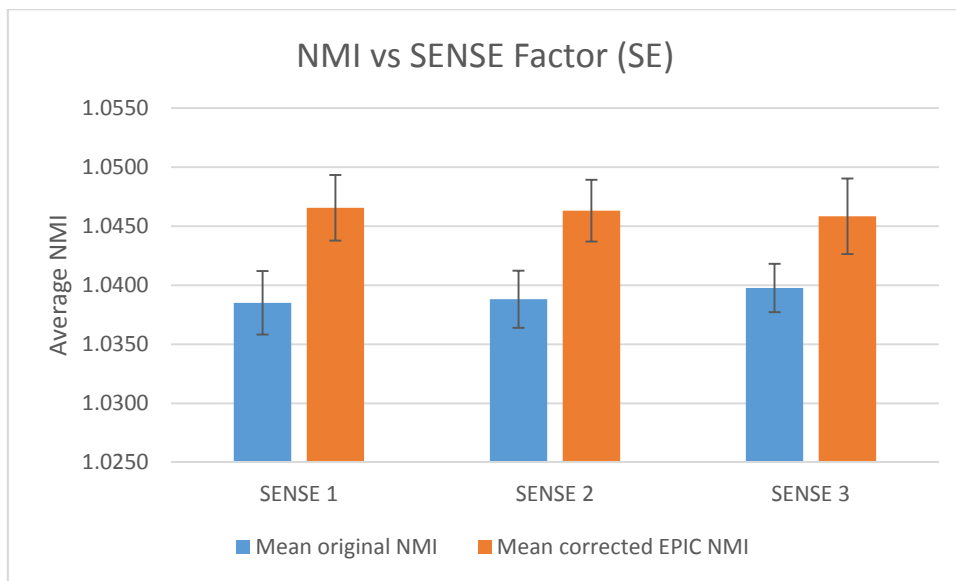


*Figure 5.34 The average NMI of SE-EPI images, before and after EPIC correction with varying SENSE factor*

There was found to be no significant difference between the values of change in mutual information after correction with varying SENSE factor in SE-EPI according to the Kruskal-Wallis test, however the standard deviation of the change in mutual information for SENSE factor 3 was much larger than the standard deviations for lower SENSE factor values.
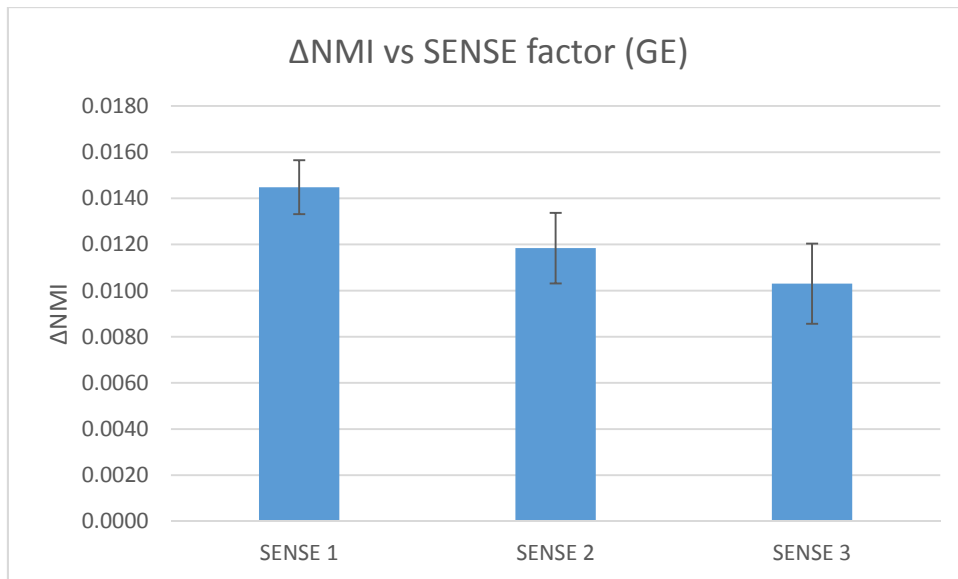
*Figure 5.34 The change in NMI of SE-EPI images after EPIC correction with varying bandwidth*



*Figure 5.35 A comparison of the three correction methods using SE-EPI images of varying SENSE factor.*

## 5.4 Slice Thickness

For the GE-EPI images, the differences in average NMI with varying slice thickness were statistically insignificant according to the Kruskal-Wallis test. We see an expected increase in NMI in the original images with respect to slice thickness.



*Figure 5.40 The average NMI of GE-EPI images, before and after EPIC correction with varying slice thickness*

The variation of the value of the change in NMI with varying slice thickness was also found to be statistically insignificant in the GE-EPI images according to the Kruskal-Wallis test. The change in NMI seems to reduce with increasing slice thickness.

*Figure 5.41 The change in NMI of GE-EPI images after EPIC correction with varying slice thickness*
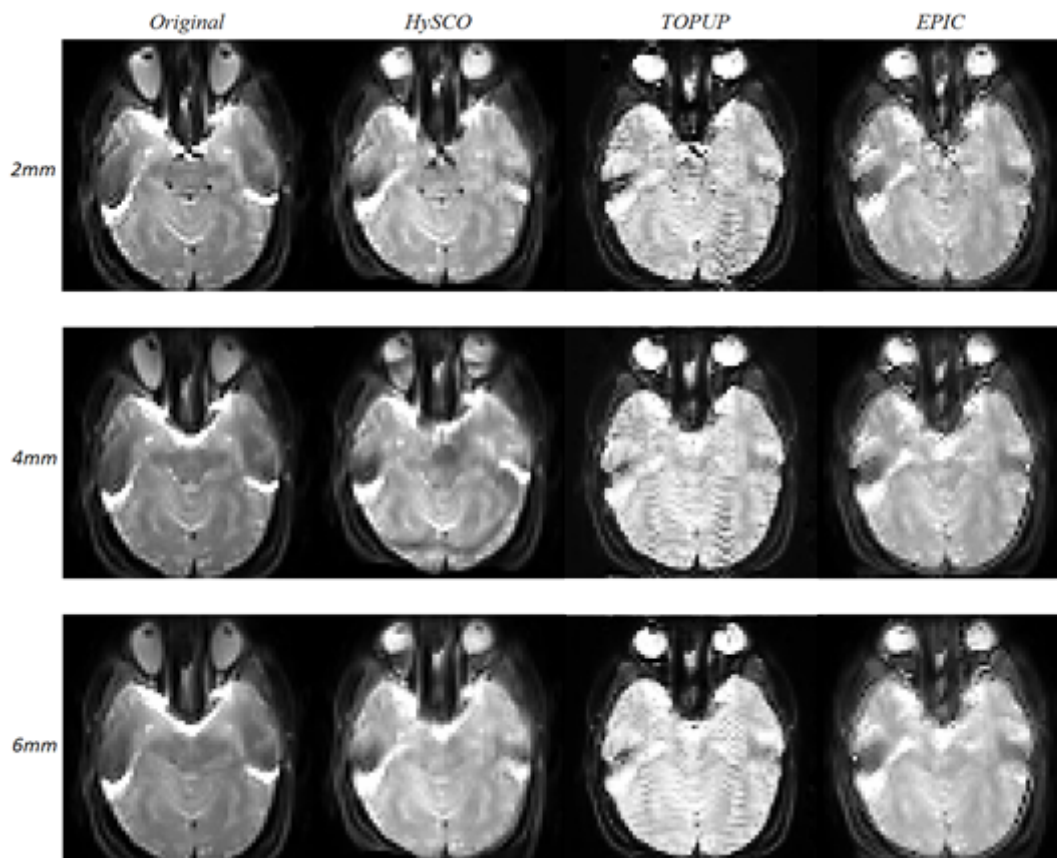


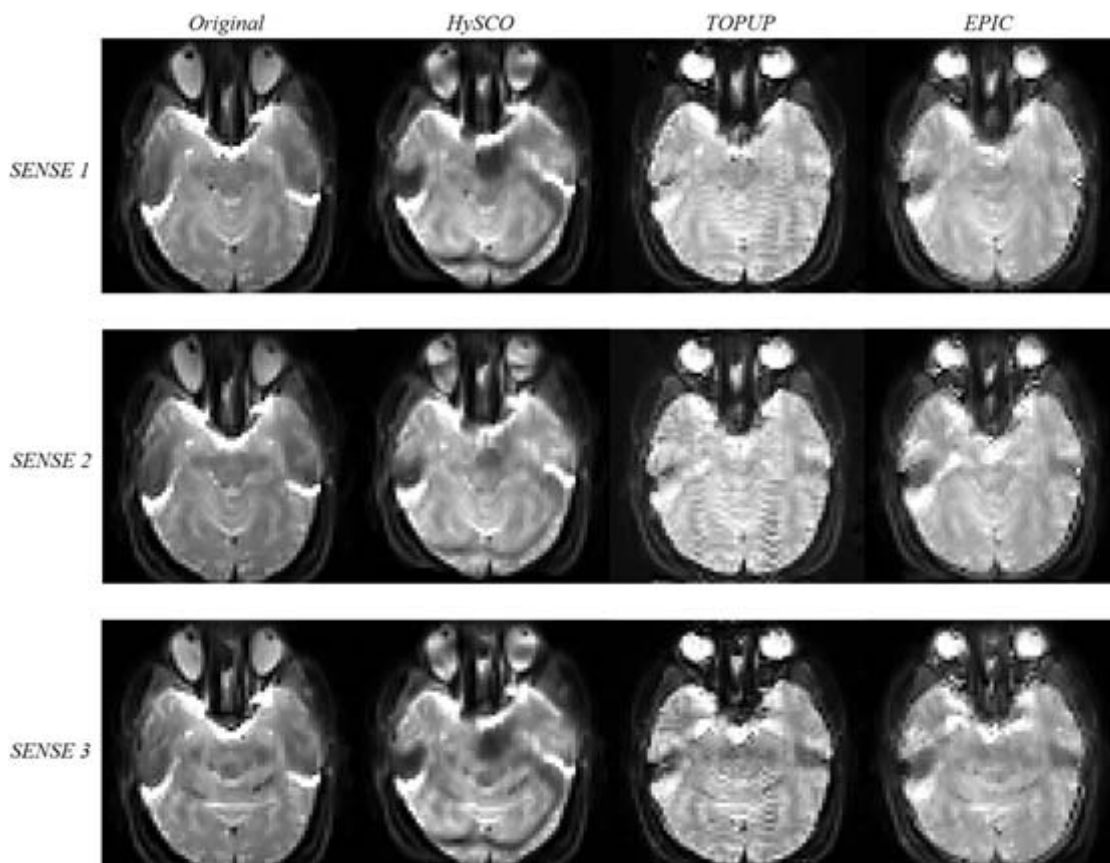*Figure 5.42 A comparison of the three correction methods using GE-EPI images of varying slice thickness.*

For the SE-EPI images, the variation of the average NMI with respect to slice thickness was statistically insignificant according to the Kruskal-Wallis test. We see a smaller increase in NMI in the original images with respect to slice thickness than in the GE-EPI images.
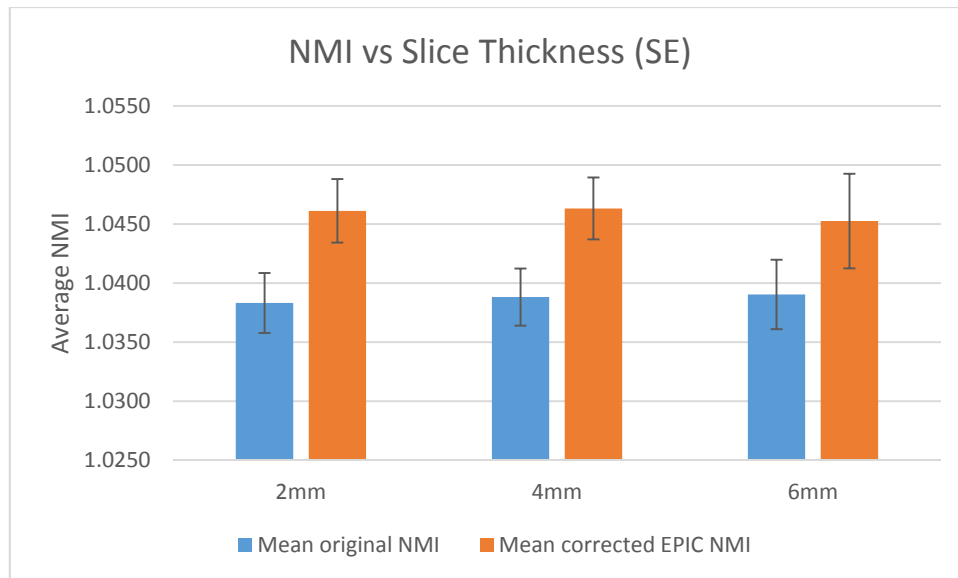


*Figure 5.43 The average NMI of SE-EPI images, before and after EPIC correction with varying slice thickness*

The variation of the change in NMI with respect to slice thickness was statistically insignificant according to the Kruskal-Wallis test for SE-EPI. The change in NMI seems to reduce with increasing slice thickness. Note that the variance of the change in NMI at 6mm slice thickness is very much higher than the others.
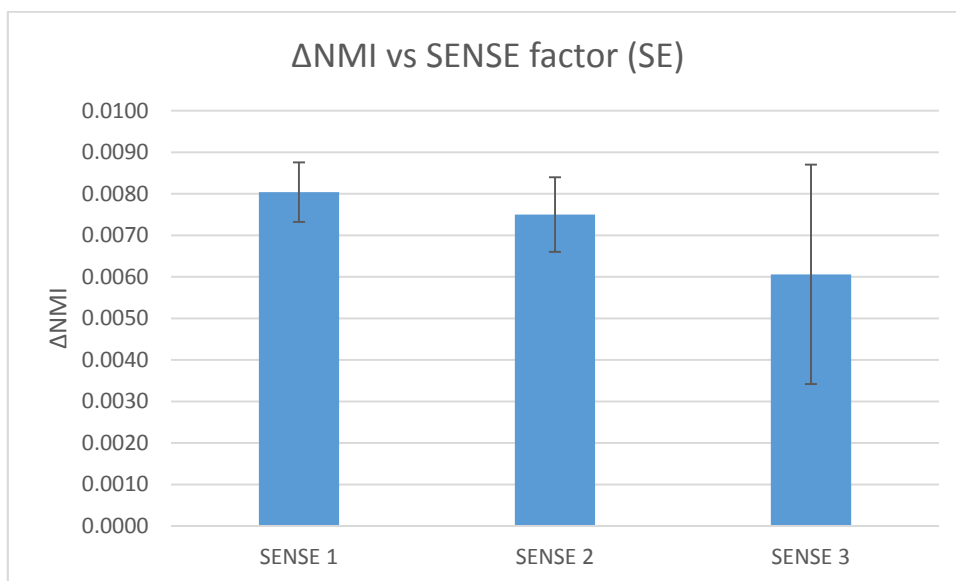
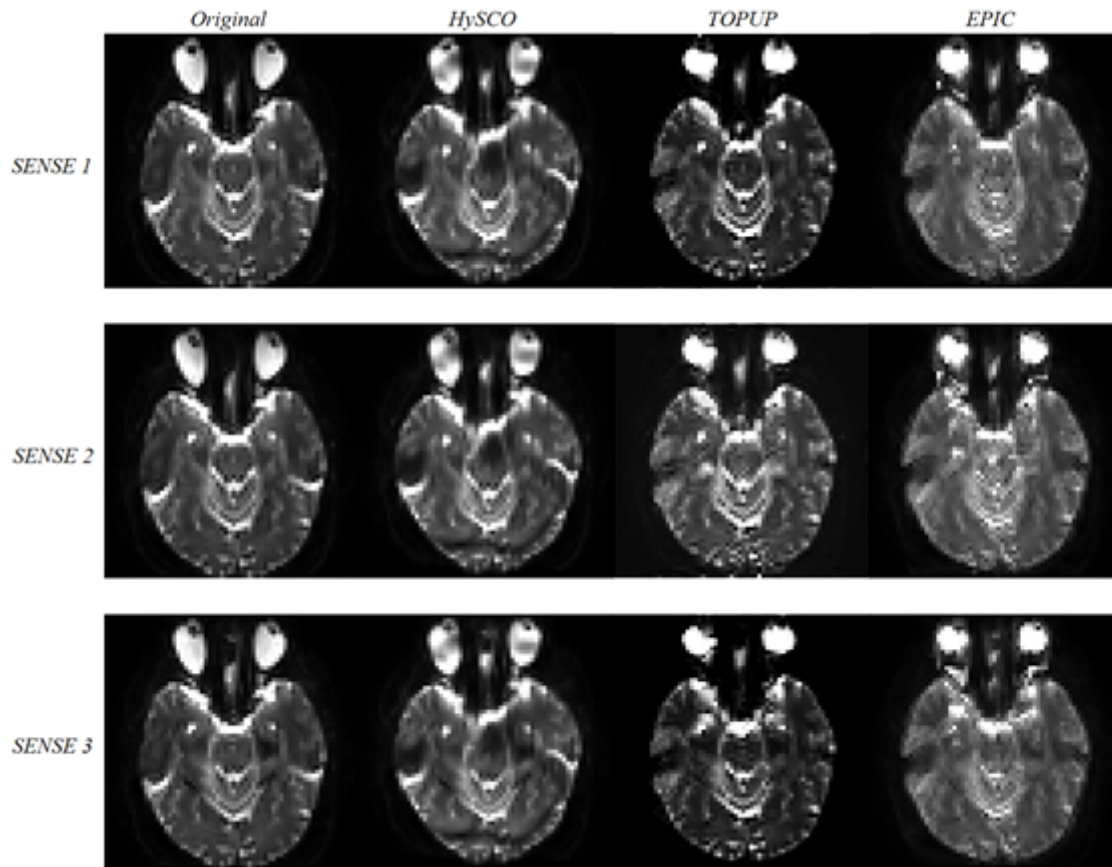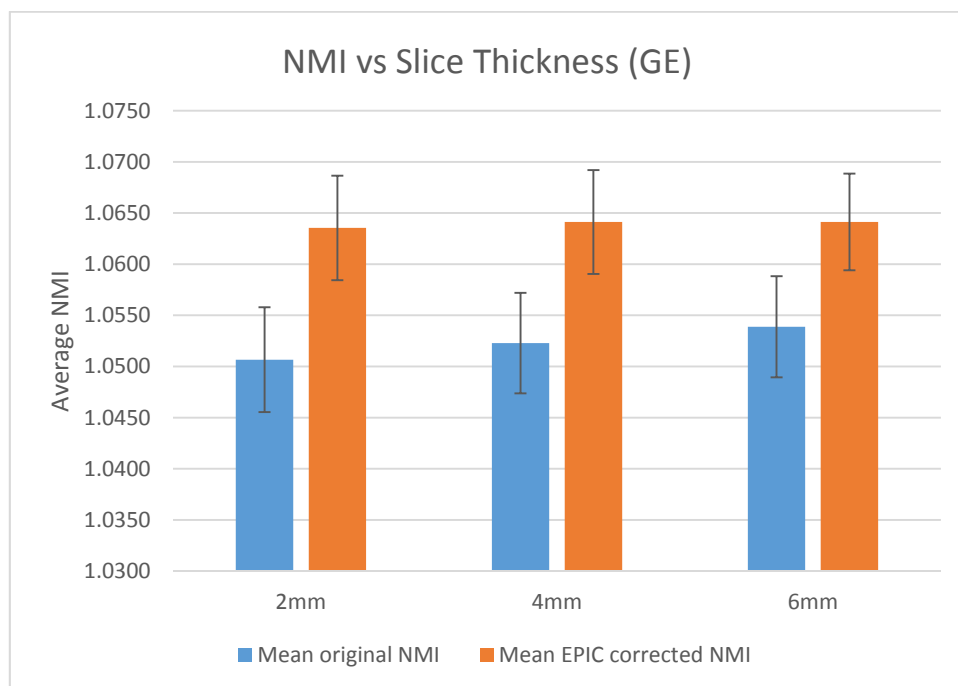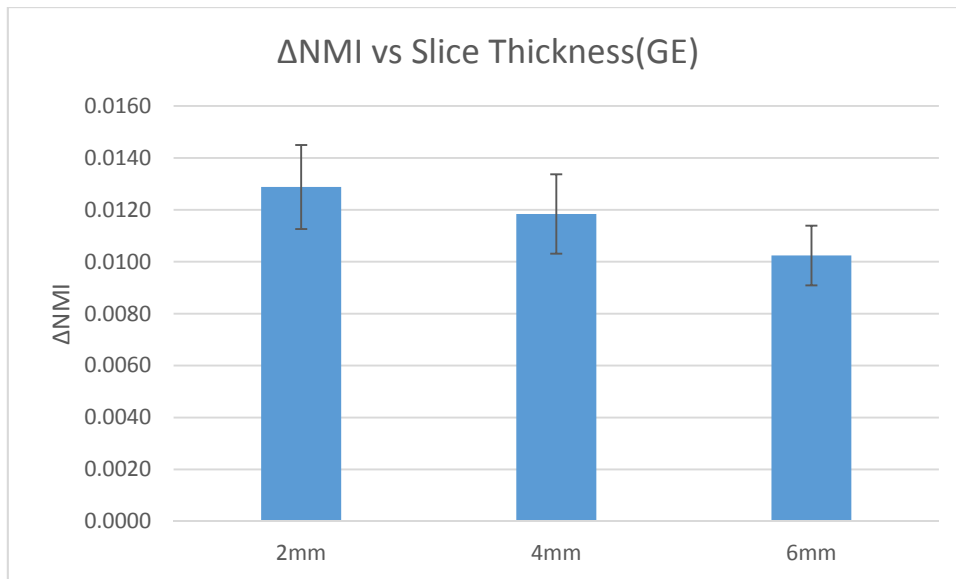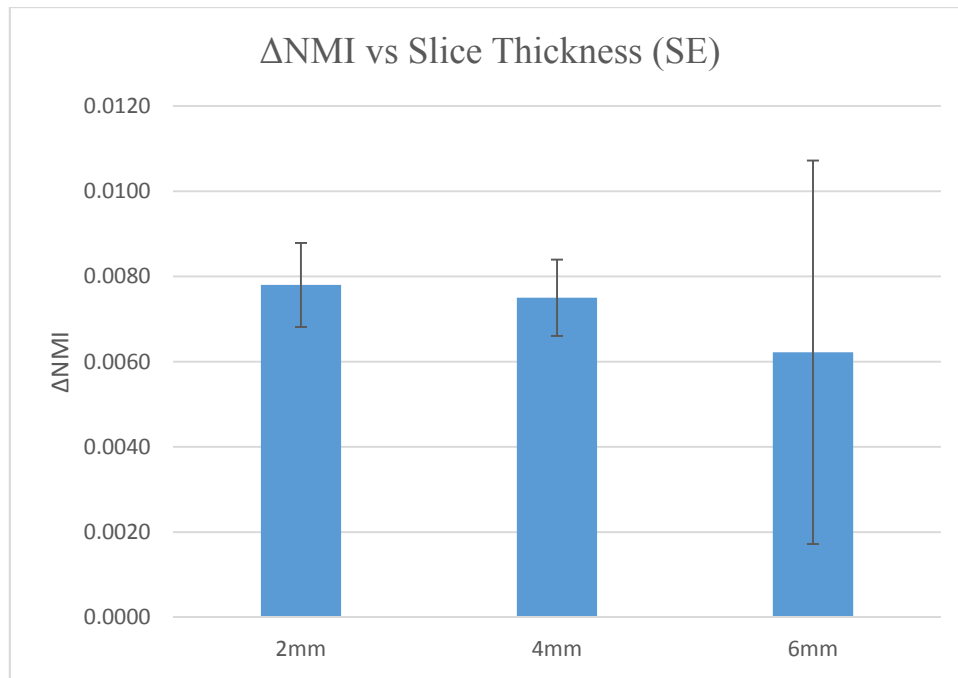*Figure 5.44 The change in NMI of SE-EPI images after EPIC correction with varying slice thickness*
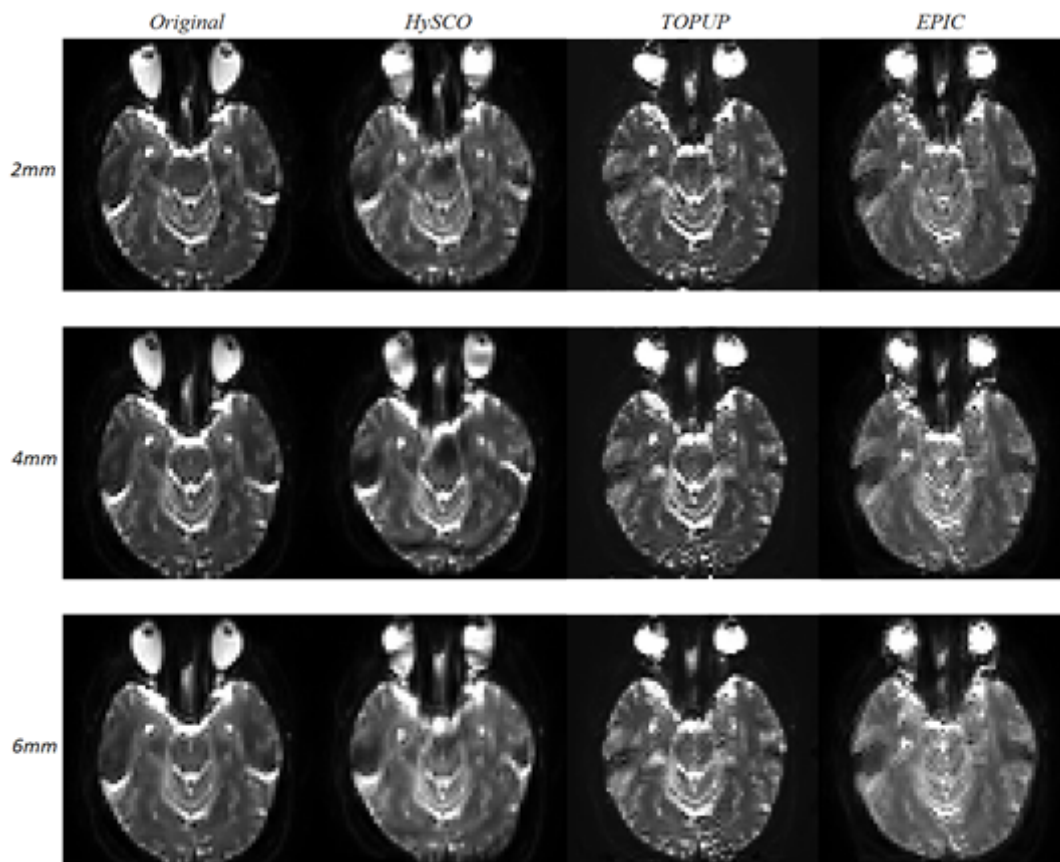


*Figure 5.45 A comparison of the three correction methods using GE-EPI images of varying SENSE factor*

## 5.5  Animal Scanner (7T) images

The images from the 7T animal scanner were successfully corrected, and showed a marked increase in NMI after correction. These results were not statistically tested as only one set of images was corrected, but the geometric distortions in the images seem to have been corrected.
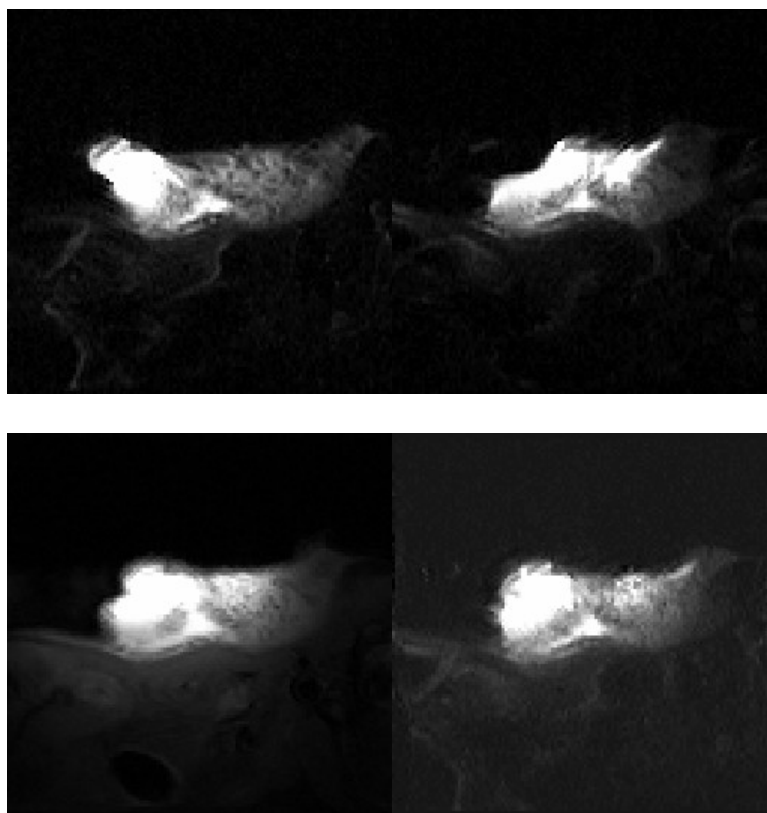


*Figure 5.41 The original single shot SE-EPI image with right-left phase encoding direction (top left), the original single shot SE-EPI image with left-right phase encoding direction (top right), the multi-shot EPI image (bottom left) and the corrected image (bottom right)*

The NMI values for the left-right (LR) phase image, the RL phase image, and the TOPUP corrected image are shown below:
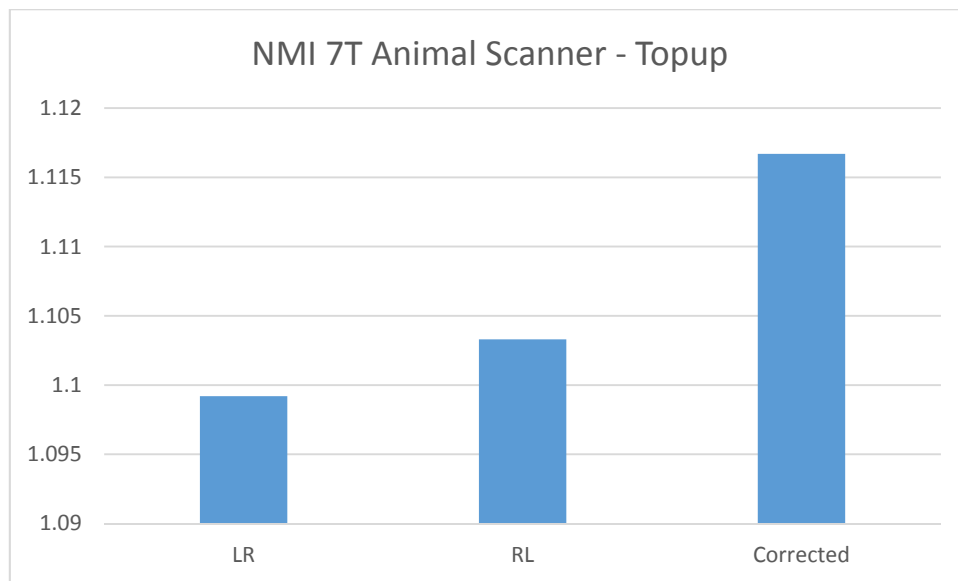


*Figure 4.42 NMI values for the uncorrected and corrected animal scanner images*

# 6 Discussion

Using NMI values obtained via cross-modality co-registration to gauge the quality of susceptibility correction is an established method for image comparison [21]. However, it would be to oversimplify to state that NMI is a single number which quantifies the quality of an image generally. Rather, it is a quantity that gives a measure how well two images are aligned. However, since all the images were co-registered prior to obtaining the value of NMI, this should provide a good indication of the level of artefacting and non-linear warping in the image. The NMI value, however, is not affected greatly by the signal to noise ratio, which is relevant to the findings with regards to the various image parameters that were investigated in this experiment. Nor is it greatly affected by the contrast to noise ratio. It is therefore that the NMI value should not be interpreted as a measure of image quality on its own.

Before comparing the quality of the corrections provided by each of these tools, it is important to note that each had customisable parameters. It is therefore possible that the corrections in this experiment may not represent the best corrections attainable by use of these tools. The default values were used in this experiment, as it was reasoned that this would be representative of the way the tools were most often used. It was also reasoned that changing default parameters or influencing the inputs pre-correction would lead to a less fair comparison.

The most significant result obtained in this experiment was the discrepancy between the effectiveness of the three correction methods. EPIC consistently

showed the best performance, both in terms of the measured increase in mutual information and in terms of the visual reduction of artefacts. This result could prove important in establishing protocols for susceptibility correction in research and in the clinic. EPIC does suffer from certain limitations, however. There is no method referred to in any of the EPIC documentation for choosing an alternate phase direction than the y-direction (or the anterior-posterior direction with regards to this study). It is indeed often the case that the phase encoding direction is chosen to be the y-direction, however there are many images where this is not the case. In this respect, TOPUP and HySCO offer more flexibility without the need to manually rotate images to the xy-plane.

The TOPUP sequence was found to destroy or entirely eliminate data from the top and bottom slices in the process of correcting the images. There are two solutions suggested to eliminate this problem; either adding duplicate slices to the top and bottom of the 3D volume, or to add empty slices to the top and bottom of the 3D volume. The former of these two methods was chosen, as this is the method EPIC chooses to solve this issue. We believe that this is an issue related to the boundary conditions of the interpolation used in the correction. TOPUP also requires that the input volume has an even number of slices. If this is not the case, it is recommended to pad the z-boundaries with an additional duplicate slice. No duplicate slices were added in the correction of the TOPUP images to provide a fair comparison with the other correction tools. Duplicate slices were added during a second TOPUP correction, however, and it was found that there was no increase in NMI, but the outside slices were preserved. Correcting images with TOPUP also lead to rippling patterns appearing on the lower bandwidth images. We are currently unaware as to why this should be the case, but it could be postulated that as the artefacts appeared in the lower bandwidth images, it could be that TOPUP struggles to correct geometric distortions that involve pixel shifts over a long distance.

HySCO was found to be the easiest correction software to implement, but unfortunately provided corrections which, for the most part, were visibly sub-par. The images suffered from blurring near areas with high field inhomogeneity and large bands of signal loss which worsened with increasing bandwidth.

The average NMI seemed to increase with increasing bandwidth. This observation agreed with our predictions, as it is known that geometric distortions become larger with lower pixel bandwidth. An interesting result, however, was that the susceptibility correction seemed to narrow the gap between the levels of mutual information for each value of bandwidth, i.e. there was more mutual information recovered from the low bandwidth images than from the high bandwidth images. This was confirmed when the correlation between the bandwidth and the change in NMI was found to be insignificant after statistical testing. This indicates that susceptibility correction can reduce the impact of bandwidth on the anatomical accuracy of EPI images. It should be noted that images with low bandwidth have a higher signal to noise ratio, and ergo susceptibility correction could be a determining factor in the optimisation of EPI sequences with regard to balancing SNR and the impact of geometric distortions.

The variation in average NMI with respect to SENSE factor was insignificant according to the Kruskal-Wallis test. However, there was a correlation between the SENSE factor and the change in NMI with correction. It was found that the gain in mutual information was inversely proportional to the SENSE factor. This could be due to susceptibility effects hindering the SENSE reconstruction process, or that due to the decreased geometric distortion, there was less to correct, as the average NMI was around equal for all levels of SENSE post-correction. In the corrected images, however, a greater extent of signal loss was found in the corrected images with higher SENSE factor. This could, once

again, be due to the detrimental effects field inhomogeneities can have on SENSE reconstruction.

The difference in the average NMI with respect to slice thickness was also found to be insignificant according to the Kruskal-Wallis Test. There are also few differences visible in the images, aside from blurring in the images with larger slice thickness. This, however, can be explained without reference to susceptibility, as with larger slices, the signal in each voxel is an average of the signal over a greater depth, thereby decreasing resolution. SNR is also dependent upon slice thickness, and therefore, from our results, it could be recommended that SNR and resolution are more important determining factor in the selection of the optimal slice thickness than any effect this parameter may have on susceptibility artefacts.

The subject was limited by the number of subjects studied. A sample size of five proved insufficient for a robust statistical analysis of the effect of scan parameters on the average NMI or the change in NMI. The default parameters for each correction method were used to ensure a fair comparison, but varying the correction parameters could have a significant impact on the quality of correction. Therefore we cannot compare the correction methods effectiveness as a whole, and the optimisation of these methods could be a topic for future research. As this research was conducted on healthy volunteers, there could be no direct assessment of the influence of correction on diagnostic efficacy. This could have been achieved by scanning patients with brain tumours and counting the number of significant normalised cerebral blood volume pixels from perfusion maps in the tumour region of interest [23]


Perhaps the most significant result was that there was very little difference in the artefacts found in our GE and SE sequences. We found no additional signal

loss in the GE images, which we expected to find due to the aforementioned T2* effects. The NMI values differed greatly between GE and SE-EPI, but this is most likely due to the difference in contrast, as both image types were compared with a T1 anatomical scan to calculate the NMI values.  Overall, the corrections were similar and equally effective in both SE and GE-EPI, which is an important finding since GE-EPI is widely used for perfusion assessment in brain tumor patients where geometric accuracy is of great importance. The results therefore warrant further testing of these correction methods in clinical situations using perfusion MRI data from brain tumor patients.

# 7 Conclusion

The various correction tools used in this experiment have been compared and the EPIC correction tool was found to provide the largest gains in mutual information whilst minimising visual artefacts in the output images. Our results indicate that susceptibility correction helps to negate the geometric distortions created in low bandwidth EPI images and acts to minimise the difference in mutual information between images of varying bandwidth. Slice thickness and SENSE factor were found to have less impact on the NMI before or after correction, but on visual inspection of the corrected images, susceptibility correction appeared to be more effective for images with lower SENSE factor. Repeating this experiment with a larger sample size could help to establish a stronger correlation between the parameters investigated and the change in NMI. The changes in NMI seemed to reflect the quality of the correction after visual inspection and therefore appears to be a good measure of anatomical accuracy. There were no major differences between the effectiveness of the corrections of GE and SE-EPI images, which is positive, as it is often stated that geometric correction is not sufficient in correcting GE-EPI images.

# 8  Bibliography

[1] Essig M. et al. (2013) Perfusion MRI: The Five Most Frequently Asked Technical Questions

[2] Riedy, G. Barker, P. (2003) Minimization of Frontal Lobe Susceptibility Artifacts in Single-Shot Echo-Planar Imaging at 3 T

[3] Bhushan, C. et al. (2012) Correcting Susceptibility-Induced Distortion in Diffusion-Weighted MRI using Constrained Nonrigid Registration

[4] Esteban, O. et al. (2014) Simulation-Based Evaluation of Susceptibility Distortion Correction Methods in Diffusion MRI for Connectivity Analysis

[5] EPI Pulse Sequence, n.d. diagram, viewed 4 June 2015, http://www.humanconnectome.org/about/project/pulse-sequences.html

[6] Ramalho, S. S. et al. (2000) Images by Nuclear Magnetic Resonance. A Modified Version of the EPI Method www.scielo.br/scielo.php?script=sci_arttext&pid=S0103-97332001000200025

[7] Holland, D. et al. (2010) Efficient correction of inhomogeneous static magnetic field-induced distortion in Echo Planar Imaging

[8] Zeng, H. and Constable, R. T. (2002) Image Distortion Correction in EPI: Comparison of Field Mapping With Point Spread Function Mapping

[9] S.M. Smith et al. (2004) Advances in functional and structural MR image analysis and implementation as FSL

[10] J.L.R. Andersson, S. and Skare, J. Ashburner (2003) How to correct susceptibility distortions in spin-echo echo-planar images: application to diffusion tensor imaging

[11] Ruthotto et al. (2012) Diffeomorphic susceptibility artifact correction of diffusion-weighted magnetic resonance images

[12] Ruthotto et al. (2013) HySCO - Hyperelastic Susceptibility Artifact Correction of DTI in SPM

[13] Modersitzki, J. (2009) FAIR: Flexible Algorithms for Image Registration

[14] Weiskopf, N et al. (2006) Optimal EPI parameters for reduction of susceptibility-induced BOLD sensitivity losses: A whole-brain analysis at 3 T and 1.5 T

[15] Knipe, H et al. Diffusion Weighted Imaging, viewed 4 June 2015, http://radiopaedia.org/articles/diffusion-weighted-imaging-1

[16] Andersson, J. L. R. et al. (2003) How to correct susceptibility distortions in spin-echo echo-planar images: application to diffusion tensor imaging

[17] Posse, S. and Aue, W. P. (1990) Susceptibility Artifacts in Spin-Echo and Gradient-Echo Imaging

[18] Bjørnerud, Atle (2008) The Physics of Magnetic Resonance Imaging

[19] Yanasak, N. E. and Kelly, M. J. (2013) MR IUmaging Artifacts and Parallel Imaging Techniques with Calibration Scanning: A New Twist on Old Problems

[20] Port, J. D. and Pomper, M. G. (2000) Quantification and Minimization of Magnetic Susceptibility Artifacts on GRE Images

[21] Fritz, L. et al. (2014) Comparison of EPI distortion correction methods at 3T and 7T

[22] SPM, http://www.fil.ion.ucl.ac.uk/spm/

[23] Vardal, J (2014) Correction of B0-Distortions in Echo-PlanarImaging–Based Perfusion-Weighted MRI

[24] FMRIB Software Library, http://fsl.fmrib.ox.ac.uk/fsl/fslwiki/

# Appendix 1 – TOPUP

TOPUP is one of the FSL suite of software tools for MRI analysis that can be installed on a Linux machine or a virtual machine within Mac OS X or Windows. TOPUP has no GUI and therefore must be called from the command line. Here is a typical example of a call to TOPUP:

topup --imain=all_my_b0_images.nii --datain=acquisition_parameters.txt --config=b02b0.cnf –out=my_output

where the "imain" parameter is used to specifyname of the input file and where the example file "all_my_b0_images.nii" contains image volumes with opposing phase encoding directions merged into a single 4D nifti file. This merging can be achieved by using the FSL tool "fslmerge" as shown:

fslmerge -t  all_my_b0_images.nii   blip_up_volume   blip_down_volume

where the first argument designates the title for the merged image output file, and the following arguments are the files to be merged. The modifier -t is to specify that the images are to be merged as a 4D volume, rather than merging them in z direction, for example.

It is important to note that the original image volumes of opposing phase encoding direction must be 3D volumes, and therefore 4D volumes may need to be split into 3D volumes using the fslsplit command.

The datain parameter is used to point to the file containing information regarding both the phase encoding direction. Each line in this file contains four numbers. The first three are used to specify the phase encoding direction of the image volume, the numbers corresponding to the x, y and z directions respectively. The fourth number is the readout time, which need only be used if:

1) The different volumes in imain have different readout times

2) The estimated must be scaled correctly to Hz

I any other case, this value can be set to 1.

A typical datain file may be written as follows:


0 1 0 0.067

0 -1 0 0.067


This specifies that the first image acquisition used a phase encoding gradient in the positive y direction and readout time of 0.067s, and the second image acquisition used a phase encoding gradient in the negative y direction and had the same acquisition time.


The config parameter specifies the location of the file containing more advanced correction parameters, which were set to the default settings for this study. It contains such parameters as:

**subsamp** – The level of subsampling. A value of 2, for example, will collapse a 2x2x2 area to a single voxel and the transform will be calculated at this scale. This is then normally repeated for smaller levels of subsampling until full resolution, given by a value of 1

**warpres** – The resolution of the warps in mm for each subsampling level. The warp resolution should normally be set to the voxel size, indicating one spline per voxel. To do this, the value must be equal to twice the smallest voxel dimension.

**fwhm** – The full width half maximum used in the Gaussian smoothing process for each subsampling step. This normally is set to 0 for the last subsampling level, eliminating smoothing.

**minmet** – chooses the method used to solve for least squares for each subsampling level. A value of zero will specify the use of the Levenberg-Marquardt algorithm, whereas a value of 1 will specify the use of the scaled conjugate gradient method.

**miter** – The maximum number of iterations per sub-registration. This is dependent on the value of minmet used. For minmet=0 we require fewer iterations than for minmet=1.

**lambda** – The relative weight of regularisation, normally having descending value for each level of subsampling. This value acts to prevent overfitting, particularly in the earlier, less accurate passes with higher values of subsampling.

**estmov** – Toggles movement correction. A value of one will allow topup to estimate the movement between acquisitions as well as correct susceptibility artefacts.

The above parameters can require several values, indicating the parameters used for each pass of the correction algorithm for each level of sub-sampling. The following values require only single values:

**ssqlambda** – If set to one, the value of lambda is multiplied by the current average squared difference. This scales the weight of regularisation appropriately for each subsampling step; higher for early iterations, lower for the later iterations.

**regmod** - Specifies the regularisation model used, and has values of either "bending_energy" or "membrane_energy". This affects the weight of regularisation per value of lambda, and higher lambda values may be necessary when using the bending energy regularisation model.

**splineorder** – Specifies whether cubic or quadratic splines should be used to model the off resonance field. While using quadratic splines use less memory and allows the hessian matrix to be calculated faster, its use may introduce incompatibilities with the bending energy regularisation model, hence cubic splines being used as default

**numprec** – This determines how precisely the Hessian matrix is calculated and stored, determining how much RAM is needed to store the hessian matrix.

**interp** – Specifies the type of interpolation used, namely linear or spline interpolation. Spline interpolation is generally more accurate, but takes longer to calculate.

**scale** – If given a value of 1, this parameter scales the intensity of each image to the common mean intensity of the images. This is not required if all acquisitions were calibrated using the same calibration scan.

**regrid –** when set to the default value of 1, registration is performed using a different grid-spacing than the input images.

All of the config file values can also be specified in the command line, which take precedence over the values set in the configuration file.

The out parameter specifies the name of the output standard output files. These files include a move parameters text file, which gives a representation if the estimated patient movement in matrix form, and a field coefficients file, which is a nifti file which shows the spline coefficients of the estimated field.

The fout parameter is optional and provides an additional representation of the fieldmap in the output scaled to Hz.

The iout parameter is used predominantly to check if the field was estimated correctly by providing movement and susceptibility correction of the input image volumes. This correction is not as robust as that provided by applytopup and is used mainly for sanity-checking.

"applytopup" is then used to take the output from the out parameter of the topup command and apply it to other images. It has proven difficult to correct dynamic series with applytopup directly, and therefore implementing a loop using a shell script is recommended for batch corrections.

A typical call to applytopup is of the form:

applytopup --imain=my_blipup1,my_blipup2 --datain=my_parameters --inindex=1,2 --topup=my_field --out=my_good_images

where imain specified the input files to be corrected. The output will average the images in the input, but a single image can be used by using the Jacobian interpolation method and using only the filename of the file to be corrected as the -imain parameter.

# Appendix 2 – EPIC

EPIC is a Linux based software and ergo was installed on a Linux virtual machine for the purposes of this project. It, similarly to TOPUP, has no GUI and must be called from the command line.

Before using EPIC for the first time, it is necessary to convert the image volumes to be corrected to the mgz file type. In this experiment, Freesurfer tools were used to convert our nifti files to mgz files, namely the mri_convert command, which can be called as follows:

mri_convert --in_type nii --out_type mgz --input_volume nifti_volume_name --output_volume mgz_volume_name

where "in_type" specifies the file type to be converted, "out_type" specifies the desired output file type, input_volume specifies the name of the file to be converted and output_volume specifies the name of the converted output file.

Once both the forward and reverse phase encoding direction volumes are converted, EPIC can be called from the command line as follows:

epic -f mgz_PA_direction  -r mgz_AP_direction -od output_directory

where the -f parameter specifies the image with forward (PA) phase encoding direction, -r specifies the image with reverse (AP) phase encoding direction, and od specifies the full path of the output directory.

There are many other parameters which parallel the similar parameters in topup:

defaults – lists the default parameters

ip – points to an input parameters file

fo – specifies the forward image correction output directory

ro – specifies the reverse image correction output directory

di – specifies a displacement field input (used later in applyEPIC)

do – specifies filename for the displacement field output

voxStep - An integer value determining how many voxels are sampled in each dimension. A value of 3, for example, would only sample every 3rd voxel in each dimension.

nchunksZ – This parameter determines how to divide the image in the z-direction for processing.

scaleImages – Determines the whether the images are scaled to the value of imageMax

imageMax – Sets the maximum pixel value

kernelWidthMax – Determines the width of the Gaussian smoothing kernel, must be an odd number of three or greater or zero.

nvoxNewZbdry – Adds additional layers to either side of the image in the z-dimension. These additional slices are duplicates of the first and last 2D images in the z-direction.

lambda1 – Sets the value of the coefficient of displacement normalisation used for the cost function. Must be a value greater than one.

lambda2 - Sets the value of the coefficient of the coefficient of the gradient used for the cost function. Must be a value greater than one.

lambda2P - Sets the value of the coefficient of  the alternative gradient used for the cost function. Must be a value greater than one.

On completion of the epic correction, 5 output files are obtained; one correction for each input image, an average of these two images, the displacement field, and the displacement field scaled to Hz.

Bear in mind, phase encoding direction must be in y, there is no clear documentation on changing the phase direction provided with this software.

On obtaining the displacement field, this can be used to correct other images using the applyEpic command. This has the same command has the same arguments above, except for one additional parameter –d which specifies the

displacement field to be used. A simple example of a call to applyEpic is as follows:

applyEpic –f PA_image_warped –d disp_field.mgz

The output of which gives the corrected image.

# Appendix 3 – HySCO

HySCO is run directly from the SPM GUI within MATLAB. Upon running SPM, HySCO can be opened via the tools tab in the batch editor. This brings up various options:

•       "Reference blip-up image", where a distorted PA image is selected from which the warp map is to be calculated.

•       "Reference blip-down image", where a distorted AP image is selected from which the warp map is also to be calculated.

•       "Other blip-up images", which is used to select other PA images to be corrected

•       "Other blip-down images", which is used to select other AP images to be corrected

•       "Dimension of phase-encoding", allowing values of "x","y", or "z"

- "Maximal Data resolution", which is used to choose the discretisation level for the estimation of the field inhomogeneity. Takes values of "full" or "half"

- "Apply to other images", which allows the user to decide whether to use the same warp map for all corrections or to generate a new warp map for each pair of images.

- "Smoothing of spline-interpolation", allows for optimisation of noise by choosing between standard cubic B-spline interpolation without smoothing or varying degrees of smoothing.

- "Weight for "diffusion" regulariser" is another smoothing parameter. Large values give more smoothing, but the corrected images will differ more than for lower values.

- "Weight for "Jacobian" regularizer" determines the maximum level of compression/expansion of the volume. For all positive values, the transformations will be invertible

After running the correction, warp maps will be generated and unwarped images will be obtained for each forward and reverse phase encoded image volume.